REPORT 1123

A STUDY OF INVISCID FLOW ABOUT AIRFOILS AT HIGH SUPERSONIC SPEEDS [1]

By A. J. Eggers, Jr., Clarence A. Syvertson, and Samuel Kraus

SUMMARY

Steady flow about curved airfoils at high supersonic speeds is investigated analytically. With the assumption that air behaves as an ideal diatomic gas, it is found that the shock-expansion method may be used to predict the flow about curved airfoils up to arbitrarily high Mach numbers, provided the flow deflection angles are not too close to those corresponding to shock detachment. This result applies not only to the determination of the surface pressure distribution, but also to the determination of the whole flow field about an airfoil. Verification of this observation is obtained with the aid of the method of characteristics by extensive calculations of the pressure gradient and shock-wave curvature at the leading edge, and by calculations of the pressure distribution on a 10-percent-thick biconvex airfoil at 0° angle of attack.

An approximation to the shock-expansion method for thin airfoils at high Mach numbers is also investigated and is found to yield pressures in error by less than 10 percent at Mach numbers above 3 and flow deflection angles up to 25°. This slender-airfoil method is relatively simple in form and thus may prove useful for some engineering purposes.

Effects of caloric imperfections of air manifest in disturbed flow fields at high Mach numbers are investigated, particular attention being given to the reduction of the ratio of specific heats. So long as this ratio does not decrease appreciably below 1.3, it is indicated that the shock-expansion method, generalized to include the effects of these imperfections, should be substantially as accurate as for ideal-gas flows. This observation is verified with the aid of a generalized shock-expansion method and a generalized method of characteristics employed in forms applicable for local air temperatures up to about 5,000° Rankine.

The slender-airfoil method is modified to employ an average value of the ratio of specific heats for a particular flow field. This simplified method has essentially the same accuracy for imperfect-gas flows as its counterpart has for ideal-gas flows.

An approximate flow analysis is made at extremely high Mach numbers where it is indicated that the ratio of specific heats may approach close to 1. In this case, it is found that the shock-expansion method may be in considerable error; however, the Busemann method for the limit of infinite free-stream Mach number and specific-heat ratio of 1 appears to apply with reasonable accuracy.

INTRODUCTION

Small-disturbance potential-flow theories have been employed widely, and for the most part successfully, for predicting the pressures (and velocities) at the surface of an airfoil in steady motion at low supersonic speeds. Thus the linear theory of Ackeret (ref. 1) has proven particularly useful in studying the flow about relatively thin, sharp-nosed airfoils at small angles of attack, while the second-order theory of Busemann (ref. 2) has found application when thicker airfoils at larger angles of attack were under consideration. At high free-stream Mach numbers the range of applicability of any potential theory is seriously limited, however, due to the production of strong shocks by even the relatively small flow deflections caused by thin airfoils. The assumption of potential flow is invalidated, of course, by the pronounced entropy rises occurring through these shocks.

This limitation on potential theories was early recognized and led to the adoption (see ref. 3) of what is now commonly called the shock-expansion method. The latter method derives its advantage over potential theories, principally, by accounting for the entropy rise through the oblique shock emanating from the leading edge of a sharp-nosed airfoil. Consequently, so long as the disturbed air behaves essentially like an ideal gas, and so long as entropy gradients normal to the streamlines (due to curvature of the surface) do not significantly influence flow at the surface, the shock-expansion theory should predict the pressures at the surface of an airfoil with good accuracy—it is tacitly assumed, of course, that the flow velocity is everywhere supersonic, and that the Reynolds number of the flow is sufficiently large to minimize viscous effects on surface pressures.

The departure of the behavior of air from that of an ideal gas at the temperatures encountered in flight at high supersonic speeds has been the subject of some investigation in the case of flows through oblique shock waves. In reference 4, the effects of thermal and caloric imperfections on the pressure rise across an oblique shock wave were investigated at sea-level Mach numbers of 10 and 20, and it was found that these effects decreased the rise by less than 5 percent for maximum temperatures up to 3,000° R. (corresponding to flow deflection angles up to 24°). This decrease was found to be due almost entirely to caloric imperfections, or changes in vibrational heat capacities of the air passing through the shock wave. The changes in temperature and density of the air passing through the wave were affected to a considerably greater extent. Subsequently, an investigation was carried out by Ivey and Cline up to Mach numbers as high as 100 (ref. 5), using the results for normal shock waves obtained by Bethe and Teller considering effects of dissociation (ref.

[1] Supersedes NACA TN 2646, "Inviscid Flow About Airfoils at High Supersonic Speeds" by A. J. Eggers, Jr., and Clarence A. Syvertson, 1952, and NACA TN 2729 "An Analysis of Supersonic Flow in the Region of the Leading Edge of Curved Airfoils, Including Charts for Determining Surface-Pressure Gradient and Shock-Wave Curvature" by Samuel Kraus, 1952.

6). As would be expected, the pressures were found to be affected to a somewhat greater extent at the higher Mach numbers.

The extent to which flow in the region of the leading edge of an airfoil departs from the simple Prandtl-Meyer type has also been investigated at high supersonic airspeeds. If the surface is curved, for example, to give an expanding flow downstream of the leading edge, expansion waves from the surface will interact with the nose shock wave, thereby curving it and yielding a nonisentropic flow field. This flow field may be characterized not only by disturbances emanating from the surface but also by disturbances reflecting to some extent from the shock wave back toward the surface. The manner in which these phenomena dictate shock-wave curvature and surface pressure gradient in ideal-gas flows at the leading edge has been treated by Crocco (ref. 7) and more recently by Schaefer (ref. 8), Munk and Prim (ref. 9), Thomas (ref. 10), and others. In the cases considered by Munk and Prim, it was found that surface pressure gradients were less (in absolute value) than those obtained assuming Prandtl-Meyer flow at the higher Mach numbers (i. e., Mach numbers greater than about 3) although, generally, by no more than about 10 percent. Since curved airfoils are likely to be of fundamental interest at high flight speeds (see, e. g., ref. 11), the effects of reflected disturbances would appear to merit further investigation, both at the leading edge and as regards their influence on the whole flow field. In addition, it would appear desirable to consider effects of gaseous imperfections through the field.

Such an investigation has therefore been undertaken in the present report, using the method of characteristics to obtain accurately flow fields and as a basis for obtaining the more approximate methods of analysis. The method is employed in a generalized form which allows caloric imperfections, as well as entropy gradients, in the flow to be considered at temperatures up to the order of 5,000° R.—thermal imperfections are neglected (see ref. 4). A 10-percent-thick biconvex airfoil is treated at Mach numbers from 3.5 to infinity, and the results are compared with the predictions of the shock-expansion method, including a simplified form of the method applicable to slender airfoils at high Mach numbers and a generalized form of the method including effects of caloric imperfections. In addition, flow in the region of the leading edge of curved airfoils is considered in some detail. Values of the surface pressure gradient and shock-wave curvature are presented for a wide range of Mach numbers and flow deflection angles.

SYMBOLS

a	local speed of sound
c	chord
C_1, C_2	characteristic coordinates (C_1 positively inclined and C_2 negatively inclined with respect to the local velocity vector)
c_d	section drag coefficient
c_l	section lift coefficient
c_m	section moment coefficient (moment taken about leading edge)
C_p	pressure coefficient, $\frac{p-p_0}{q_0}$
c_p	specific heat at constant pressure
c_v	specific heat at constant volume
K	curvature
M	Mach number (ratio of local velocity to local speed of sound)
P	pressure ratio, $\frac{p}{p_0}$
p	static pressure
q	dynamic pressure
R	gas constant
s, n	rectangular coordinates (in streamline direction and normal to streamline direction, respectively)
T	temperature, °R.
t	time
V	resultant velocity
W	distance measured from leading edge along airfoil surface
x, y	rectangular coordinates
α	angle of attack, radians unless otherwise specified
β	Mach angle, arc sin $\left(\frac{1}{M}\right)$, radians
γ	ratio of specific heats, $\frac{c_p}{c_v}$ (Average value of γ is γ_a.)
δ	flow deflection angle, radians unless otherwise specified
ζ	angle between shock wave and flow direction just downstream of shock wave, radians
θ	molecular vibrational energy constant, °R. (5,500° R. for air)
κ	ratio of shock-wave curvature to that given by the shock-expansion method
ρ	mass density
σ	shock-wave angle, radians
ψ	ratio of surface pressure gradient to that given by the shock-expansion method
ω	ray angle for Prandtl-Meyer flow, radians

SUBSCRIPTS

0	free-stream conditions
A,B,C,D	conditions at different points in flow field
i	ideal-gas quantities
N	conditions at the leading edge immediately downstream of the shock wave
S	conditions on streamline
w	conditions along airfoil surface
σ	conditions along shock wave

SUPERSCRIPT

$-$	vector quantities

DEVELOPMENT OF METHODS OF ANALYSIS

GENERAL METHODS

Method of characteristics.—Two-dimensional rotational supersonic flows have been treated by numerous authors with

the aid of the method of characteristics, and various adaptations of the method have been found which are especially suited for studying particular types of such flows. In the case of steady flows in which atmospheric air does not behave as an ideal diatomic gas, a very familiar and simple form of the compatibility equations may be employed. To illustrate, consider the Euler equation

$$\rho \frac{d\overline{V}}{dt} = -\text{grad } p \tag{1}$$

the continuity equation

$$\text{div } (\rho \overline{V}) = 0 \tag{2}$$

and the equation for the speed of sound (evaluated at constant entropy)

$$a^2 = \frac{dp}{d\rho} \tag{3}$$

Rewriting equations (1) and (2) in the form of partial differential equations and transforming the resulting expressions to the characteristic, or C_1, C_2, coordinate system, there is obtained, upon combination with equation (3), the following relations for steady flow:

$$\frac{\cot \beta}{\rho V^2}\left(\frac{\partial p}{\partial C_1} - \frac{\partial p}{\partial C_2}\right) + \left(\frac{\partial \delta}{\partial C_1} + \frac{\partial \delta}{\partial C_2}\right) = 0 \tag{4}$$

and

$$\frac{\cot \beta}{\rho V^2}\left(\frac{\partial p}{\partial C_1} + \frac{\partial p}{\partial C_2}\right) + \left(\frac{\partial \delta}{\partial C_1} - \frac{\partial \delta}{\partial C_2}\right) = 0 \tag{5}$$

A simple addition or subtraction of equations (4) and (5) then yields the compatibility equations (see, e. g., ref. 12)

$$\frac{\partial p}{\partial C_1} = -\rho V^2 \tan \beta \frac{\partial \delta}{\partial C_1} \tag{6}$$

and

$$\frac{\partial p}{\partial C_2} = \rho V^2 \tan \beta \frac{\partial \delta}{\partial C_2} \tag{7}$$

Now, in reference 4 both caloric and thermal imperfections of air were considered, and it was found that the latter imperfections [2] have a negligible effect on shock processes in atmospheric air. It may easily be shown that this conclusion also applies to expansion processes and, for this reason, caloric imperfections only are considered in detail in the present paper. These imperfections become significant in air at temperatures greater than about 800° R. and first manifest themselves as changes in the vibrational heat capacities with temperature. Thus, the specific heats c_p and c_v and their ratio γ for the gas also change. The equation of state remains, however,

$$p = \rho RT \tag{8}$$

and the specific heats are still related to the gas constant by the expression

$$c_p - c_v = R \tag{9}$$

[2] Thermal imperfections usually appear in the form of intermolecular forces and molecular-size effects and may be accounted for with additional terms in the equation of state.

Furthermore, it readily follows from the differential energy equation and these expressions that the speed of sound is given by the simple relation

$$a^2 = \gamma RT \tag{10}$$

Combining equations (8) and (10) and noting that $\sin \beta = a/V$ there is then obtained

$$\rho V^2 = \frac{\gamma p}{\sin^2 \beta} \tag{11}$$

Hence, on combining this equation with equations (6) and (7), it is apparent that the familiar compatibility equations

$$\frac{\partial p}{\partial C_1} = \frac{-2\gamma p}{\sin 2\beta} \frac{\partial \delta}{\partial C_1} \tag{12}$$

and

$$\frac{\partial p}{\partial C_2} = \frac{2\gamma p}{\sin 2\beta} \frac{\partial \delta}{\partial C_2} \tag{13}$$

also hold for the more general type of flow under consideration. These equations are basic, of course, to two-dimensional characteristics theory, and, as will be shown later, form a convenient starting point for developing simpler theories of two-dimensional supersonic flow.

In order to apply equations (12) and (13), it is evident that the manner in which γ and β or M are connected to p or δ must be known. Relations implicitly connecting these variables at temperatures up to the order of 5000° R may be readily obtained from the results of reference 4 by simply eliminating the terms therein accounting for thermal imperfections. Thus we have as a function of the local static temperature and free-stream conditions

$$\gamma = \gamma_t \left[\frac{1 + \left(\frac{\gamma_t - 1}{\gamma_t}\right)\left(\frac{\theta}{T}\right)^2 \frac{e^{\theta/T}}{(e^{\theta/T}-1)^2}}{1 + (\gamma_t - 1)\left(\frac{\theta}{T}\right)^2 \frac{e^{\theta/T}}{(e^{\theta/T}-1)^2}} \right] \tag{14}$$

and

$$M^2 = \frac{2}{\gamma}\left(\frac{T_0}{T}\right)\left[\frac{\gamma_0 M_0^2}{2} + \frac{\gamma_t}{\gamma_t - 1}\left(1 - \frac{T}{T_0}\right) + \frac{\theta}{T_0}\left(\frac{1}{e^{\theta/T_0}-1} - \frac{1}{e^{\theta/T}-1}\right)\right] \tag{15}$$

For isentropic flow along a streamline, the pressure is related to the temperature by the expression

$$\frac{p}{p_\sigma} = \frac{\Lambda(T_\sigma)}{\Lambda(T)} \tag{16}$$

where

$$\Lambda(T) = \frac{e^{\theta/T} - 1}{e^{\left(\frac{\theta}{T}\frac{e^{\theta/T}}{e^{\theta/T}-1}\right)}} \left(\frac{1}{T}\right)^{\frac{\gamma_t}{\gamma_t - 1}} \tag{17}$$

If there is a shock wave in the flow,[3] in particular, a nose or leading-edge shock, then the following additional relations obtained with equations (8), (10), and (15) and the conditions

[3] If there are no shock waves, then the subscript σ in equation (16) can, of course, be replaced with the subscript 0.

for continuity of flow and conservation of momentum along a streamline through the shock are also required:

$$\frac{p_0}{p_\sigma}=\frac{1}{2}\left\{(1+\gamma_\sigma M_\sigma^2)-\frac{T_0}{T_\sigma}(1+\gamma_0 M_0^2)+\sqrt{\left[(1+\gamma_\sigma M_\sigma^2)-\frac{T_0}{T_\sigma}(1+\gamma_0 M_0^2)\right]^2+4\,\frac{T_0}{T_\sigma}}\right\} \tag{18}$$

$$\sin^2\sigma=\frac{[(\gamma_\sigma T_\sigma M_\sigma^2)/(\gamma_0 T_0 M_0^2)]-1}{(\rho_0/\rho_\sigma)^2-1} \tag{19}$$

and

$$\tan\delta=\frac{1}{\tan\sigma}\frac{1}{\dfrac{\gamma_0 M_0^2}{(p_\sigma/p_0)-1}-1} \tag{20}$$

By use of the local static temperature as a parameter, the term $2\gamma p/\sin 2\beta$ in equations (12) and (13) may now be evaluated with equations (14) through (17). Equations (18) through (20) define the initial conditions downstream of a leading edge or other shock wave in the flow field. Thus, equations (12) through (20) provide all the information necessary to calculate the flow about an airfoil by means of the method of characteristics. As described in detail in Appendix A, the calculations are of three general types: (1) determination of conditions at a point in the flow field between the shock and the surface; (2) determination of conditions at a point on the surface; and (3) determination of conditions at a point just downstream of the shock. Case (1) entails the use of both compatibility equations, while case (2) entails the use of the compatibility equation for a second-family characteristic line in combination with the equation of the airfoil surface, and case (3) involves the compatibility equation for a first-family line in combination with the oblique-shock equations. With the aid of the three general types of calculations, the entire flow field about an airfoil can be built up numerically using a computing procedure working from the leading edge downstream. In cases where changes in the vibrational heat capacities with temperature are neglected, the calculations are, of course, simplified since γ of the gas can be considered constant, and temperature, pressure, and density ratios are simply the ideal-gas functions of Mach number.

Shock-expansion method.—This method of calculating supersonic flow of an ideal gas at the surface of an airfoil is well known, entailing simply the calculation of flow at the nose with the oblique-shock equations and flow downstream of the nose with the Prandtl-Meyer equations. Determination of airfoil characteristics in this manner requires only a small amount of time, of course, compared to that involved when the method of characteristics is used, hence, the advantage of the former method. The questions arise, however, as to exactly what the simplifying assumptions underlying the shock-expansion method are, and what form the method takes (for calculative purposes) when the gas displays varying vibrational heat capacities.

The matter of simplifying assumptions may perhaps best be considered by employing equations (12) and (13), the basic compatibility equations. If these expressions are resolved into the streamline direction and combined, noting that

$$\frac{\partial p}{\partial s}=\frac{1}{2\cos\beta}\left(\frac{\partial p}{\partial C_1}+\frac{\partial p}{\partial C_2}\right) \tag{21}$$

and

$$\frac{\partial \delta}{\partial s}=\frac{1}{2\cos\beta}\left(\frac{\partial \delta}{\partial C_1}+\frac{\partial \delta}{\partial C_2}\right) \tag{22}$$

there is then obtained the relation

$$\frac{\partial p}{\partial s}=\left(\frac{1-\dfrac{\partial\delta/\partial C_1}{\partial\delta/\partial C_2}}{1+\dfrac{\partial\delta/\partial C_1}{\partial\delta/\partial C_2}}\right)\frac{2\gamma p}{\sin 2\beta}\frac{\partial\delta}{\partial s} \tag{23}$$

defining the gradient of p along s. If flow along streamlines downstream of the nose is of the simple Prandtl-Meyer type, however, we have

$$\frac{\partial p}{\partial s}=\frac{2\gamma p}{\sin 2\beta}\frac{\partial\delta}{\partial s} \tag{24}$$

Hence, it is evident that the requirement for this type flow is

$$\left|\frac{\partial\delta/\partial C_1}{\partial\delta/\partial C_2}\right|\ll 1 \tag{25}$$

Equation (25) is, of course, simply an approximate statement of a well-known property of Prandtl-Meyer flows; namely, that flow inclination angles are essentially constant along first-family Mach lines. It follows from equation (12) that if equation (25) holds, then the pressures will also be essentially constant along these lines. It does not follow, however, that the Mach number will be constant or, for that matter, that the first-family characteristic lines will be straight (as is the case for isentropic expansion flows about a corner). In fact, it may easily be shown that the Mach number gradient along C_1 is proportional to the local entropy gradient normal to the streamlines and that the C_1 lines are curved according to the change in M. Thus we see that there is really only one basic assumption underlying the shock-expansion method; namely, disturbances incident on the nose shock (or, for that matter, any other shock) are consumed almost entirely in changing the direction of the shock. In this regard, it is interesting to note that the assumption of Thomas (ref. 13), that pressure is a function only of flow deflection angle and entropy, is equivalent to this assumption. It follows, of course, that the most general solution obtainable with Thomas' series representation of the pressure is that given by the shock-expansion method.

With the assumption that all disturbances incident on the shock wave are consumed, it is evident that the shock-expansion method provides a relatively simple means for calculating the whole flow field about an airfoil, including the effects of shock-wave curvature. The details of such calculations are presented in Appendix B. In general, of course, the validity of this assumption and the accuracy of the shock-expansion method can only be checked by com-

parison of calculations using this method with those using the method of characteristics.

The shock-expansion method for a calorically imperfect, diatomic gas is readily deduced from the equations previously obtained. For example, flow conditions at the leading edge of an airfoil can be evaluated with the oblique-shock-wave expressions (eqs. (18) through (20)) and the expression for conservation of energy (eq. (15)). The variation of flow inclination angle with pressure along the surface is then obtained by graphically integrating equation (24); namely,

$$\delta_S-\delta_N=\int_{p_N}^{p_S}\frac{\sin 2\beta}{2\gamma p}\,dp \tag{26}$$

where the variables γ, p, and β are evaluated using equations (14) through (17), employing the static temperature as a parameter. When extreme accuracy is not essential, this rather tedious calculation can be avoided, and a relatively simple algebraic solution of the flow downstream of the nose can be employed.[4] The details of this solution are presented in Appendix C. In the special case of flow at high supersonic speeds about slender airfoils, the whole calculation becomes particularly simple and warrants special attention.

If it is assumed that the local surface slopes are small compared to 1 and, in addition, that the free-stream Mach number is large compared to 1, it follows that σ and β are everywhere small compared to 1. In this case, equation (24) takes on the approximate form

$$\left.\frac{dp}{d\delta}\right|_S=\gamma pM \tag{27}$$

Furthermore, if it is assumed that γ is constant at an average value γ_a for a particular flow field (this assumption appears reasonable since, in the temperature range up to 5,000° R, the change in γ is less than about 15 percent), then the Mach number and pressure may be related by the simple expression

$$M=M_N\left(\frac{p_N}{p}\right)^{\frac{\gamma_a-1}{2\gamma_a}} \tag{28}$$

Equations (27) and (28) combine to yield the differential equation

$$\frac{1}{\gamma_a M_N}\left(\frac{p}{p_N}\right)^{\frac{-(\gamma_a+1)}{2\gamma_a}}d\left(\frac{p}{p_N}\right)=d\delta \tag{29}$$

which readily integrates (between N and S) to the form

$$\frac{p_S}{p_N}=\left[1-\left(\frac{\gamma_a-1}{2}M_N\delta_N\right)\left(1-\frac{\delta_S}{\delta_N}\right)\right]^{\frac{2\gamma_a}{\gamma_a-1}} \tag{30}$$

now denoting

$$\frac{\gamma_a-1}{2}M_N\delta_N=f(M_0\delta_N) \tag{31}$$

and

$$\frac{p_N}{p_0}=g(M_0\delta_N) \tag{32}$$

[4] The tabulated results of Noyes (ref. 14) may also prove useful in this case for Mach numbers up to 3.

there is obtained from the oblique-shock equations, simplified to conform with this analysis,

$$f(M_0\delta_N)=\frac{M_0^2\sigma_N^2-1}{\sqrt{\left(M_0^2\sigma_N^2+\frac{2}{\gamma_a-1}\right)\left(\frac{2\gamma_a}{\gamma_a-1}M_0^2\sigma_N^2-1\right)}} \tag{33}$$

and

$$g(M_0\delta_N)=\frac{2\gamma_aM_0^2\sigma_N^2-(\gamma_a-1)}{\gamma_a+1} \tag{34}$$

where

$$M_0\sigma_N=\frac{\gamma_a+1}{4}M_0\delta_N+\sqrt{1+\left(\frac{\gamma_a+1}{4}M_0\delta_N\right)^2} \tag{35}$$

With equations (30) through (35), the pressures on the surface of an airfoil may easily be obtained. In terms of pressure coefficient we have

$$C_p=\frac{2}{\gamma_aM_0^2}\left[\left(\frac{p_N}{p_0}\right)\left(\frac{p_S}{p_N}\right)-1\right] \tag{36}$$

or

$$C_p=\frac{2}{\gamma_aM_0^2}\left\{g(M_0\delta_N)\left[1-f(M_0\delta_N)\left(1-\frac{\delta_S}{\delta_N}\right)\right]^{\frac{2\gamma_a}{\gamma_a-1}}-1\right\} \tag{37}$$

The advantage of these slender-airfoil expressions lies, of course, in their relative simplicity and, thus, the ease of calculation which is inherent to them. It may be noted in this regard that the functions $f(M_0\delta_N)$ and $g(M_0\delta_N)$ can be calculated once and for all with equations (33), (34), and (35), provided the variation of γ_a with $M_0\delta_N$ is known. This calculation has been carried out for a constant value of γ equal to 1.4 and for average values of γ, assuming $T_0=500°$ R.[5] The results are presented in table I.

It should also be noted that the slender-airfoil expressions of the shock-expansion method satisfy the hypersonic similarity law for airfoils first deduced by Tsien (ref. 15).[6] A necessary condition for the validity of these expressions is thus satisfied; however, the accuracy of the shock-expansion method, whether for slender airfoils or otherwise, remains to be investigated.

METHODS FOR CALCULATING THE FLOW IN THE REGION OF THE LEADING EDGE

As was pointed out previously, pressure disturbances emanating from the surface of a curved airfoil interact with, and thereby curve, the leading-edge shock wave. The geometry of this phenomenon near the leading edge of a convex airfoil is illustrated in figure 1. The pressure disturbances from the airfoil (expansion waves for a convex airfoil) travel along first-family Mach lines C_1. In addition to changing the inclination of the shock wave, the interaction between these disturbances and the shock produces another system of disturbances which travel along second-family Mach lines C_2 from the shock wave to the surface.

Method of characteristics.—An exact solution for the surface pressure gradient and shock-wave curvature at the leading

[5] For a given value of T_0, T_N, to the accuracy of this analysis, is the ideal-gas function of $M_0\delta_N$. Thus, knowing T_N, γ_N can be determined. The average value of γ used is $\gamma_a=\gamma_a(M_0\delta_N)=(\gamma_N+\gamma_0)/2$.

[6] This fact was employed by Linnell (ref. 16) to obtain an expression for pressure coefficient equivalent to equation (37) for the case of constant γ and to obtain explicit solutions for the lift, drag, and pitching-moment coefficients of several airfoils at hypersonic speeds.

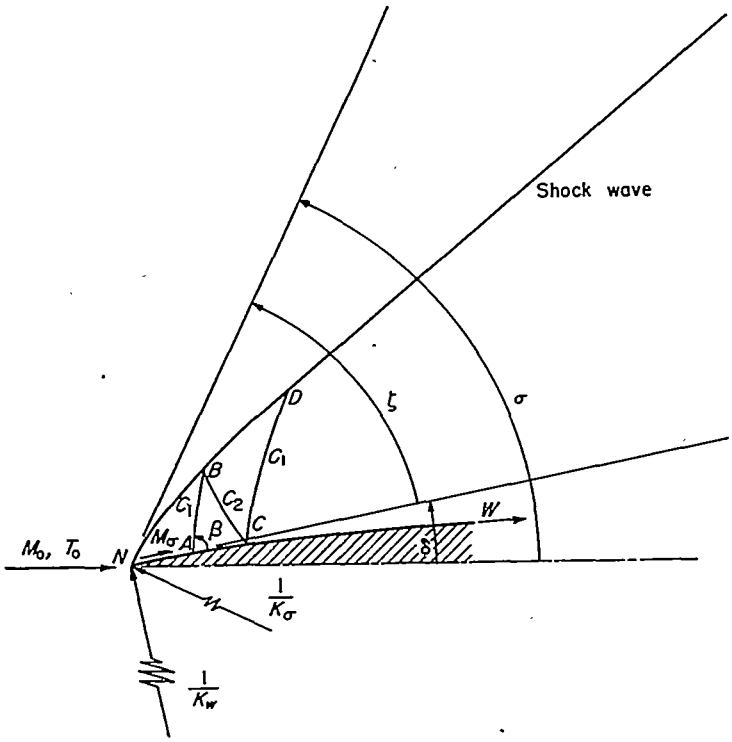

FIGURE 1.—Schematic diagram of supersonic flow past a curved sharp-nose airfoil.

edge may be determined in the following manner. It is clear, referring to figure 1, that the change in flow angle between points A and C given by the compatibility equations (see eqs. (12) and (13)) along the path ABC must equal the change determined by the airfoil surface from A to C. Similarly, the difference in pressure between points B and D given by the compatibility equations along the path BCD must equal that determined by the change in shock-wave inclination between B and D. In reference 9, these conditions were employed at the leading edge to obtain equations, in simple parametric form, for determining the surface pressure gradients and shock-wave curvatures. These equations can be written in the form

$$\frac{1}{K_w}\frac{dP}{dW}=\left(\frac{1-\frac{\partial\delta/\partial C_1}{\partial\delta/\partial C_2}}{1+\frac{\partial\delta/\partial C_1}{\partial\delta/\partial C_2}}\right)\frac{2\gamma P}{\sin 2\beta} \tag{38}$$

for the surface pressure gradient, and

$$\frac{K_\sigma}{K_w}=\frac{\sin(\beta-\sigma+\delta)+\left(\frac{\partial\delta/\partial C_1}{\partial\delta/\partial C_2}\right)\sin(\beta+\sigma-\delta)}{\left(1+\frac{\partial\delta/\partial C_1}{\partial\delta/\partial C_2}\right)\left(\frac{\partial\delta}{\partial\sigma}\right)_\sigma\sin\beta} \tag{39}$$

for the shock-wave curvature, where

$$\frac{\partial\delta/\partial C_1}{\partial\delta/\partial C_2}=\frac{\left[\frac{2\gamma P}{\sin 2\beta}-\left(\frac{dP}{d\delta}\right)_\sigma\right]}{\left[\frac{2\gamma P}{\sin 2\beta}+\left(\frac{dP}{d\delta}\right)_\sigma\right]}\left[\frac{\sin(\beta-\sigma+\delta)}{\sin(\beta+\sigma-\delta)}\right] \tag{40}$$

It should be pointed out that equation (38) is, of course, equivalent to equation (23).

A procedure for evaluating equations (38) and (39) for a calorically imperfect, diatomic gas, as well as for an ideal gas, is presented in Appendix D. Since they are exact for two-dimensional, steady, inviscid flow, values of the surface pressure gradient and shock-wave curvature at the leading edge, determined using these equations, may be put to two uses. First, the accuracy of approximate methods of calculating the flow field about a curved airfoil can be evaluated at the leading edge by comparing the values of the surface pressure gradient and shock-wave curvature predicted by these approximate methods to the values obtained using equations (38) and (39). Second, the pressure gradient and shock-wave curvature can be used to calculate the initial points of a characteristic solution for the flow about an airfoil.

Shock-expansion method.—One approximate solution for the surface pressure gradient and shock-wave curvature has already been indicated in the previous discussion of the shock-expansion method. The requirement for the application of the shock-expansion method is given by equation (25). Hence, it is apparent that under this condition the expression for the surface pressure gradient (eq. (38)) reduces to

$$\frac{1}{K_w}\frac{dP}{dW}=\frac{2\gamma P}{\sin 2\beta} \tag{41}$$

Similarly, the expression for the shock-wave curvature (eq. (39)) reduces to

$$\frac{K_\sigma}{K_w}=\frac{\sin(\beta-\sigma+\delta)}{\left(\frac{d\delta}{d\sigma}\right)_\sigma\sin\beta} \tag{42}$$

It should be realized that the flow field is determined by the basic flow equations in conjunction with the shock wave and airfoil surface as boundary conditions. Thus, the additional requirement for this shock-expansion method of zero pressure gradient along first-family Mach lines means that one of the flow relations cannot be satisfied exactly (i. e., the flow field is overdetermined). Equations (41) and (42) satisfy the shock relations and the airfoil surface as boundary conditions; however, the compatibility equations are only approximately satisfied. (See Appendix B.)

The error in surface pressure gradient associated with neglecting the reflected disturbances might be expected to be largest in the region of the leading edge of a curved airfoil due to the close proximity of the shock wave and the surface. The magnitude of the error in this region may be deduced, of course, from the ratios of values of surface pressure gradient and shock-wave curvature given by the characteristics method to those given by the shock-expansion method. The surface-pressure-gradient ratio and shock-wave-curvature ratio can be written (using eqs. (38) and (41))

$$\psi=\frac{1-\frac{\partial\delta/\partial C_1}{\partial\delta/\partial C_2}}{1+\frac{\partial\delta/\partial C_1}{\partial\delta/\partial C_2}} \tag{43}$$

and (using eqs. (39) and (42))

$$\kappa=\frac{\sin(\beta-\sigma+\delta)+\left(\frac{\partial\delta/\partial C_1}{\partial\delta/\partial C_2}\right)\sin(\beta+\sigma-\delta)}{\left(1+\frac{\partial\delta/\partial C_1}{\partial\delta/\partial C_2}\right)\sin(\beta-\sigma+\delta)} \tag{44}$$

respectively. A procedure for evaluating equations (43) and (44) for the flow of a calorically imperfect gas, as well as for an ideal gas, is presented in Appendix D. (The application of eq. (43) for an ideal gas has already been given in ref. 9.)

As was stated previously, the pressure gradient and shock-wave curvature can be used to calculate the initial points of a characteristic solution for the flow about an airfoil. It is apparent that the initial points for a shock-expansion solution can be found in a similar manner. With either type of solution, flow conditions at an initial point on the surface downstream of the leading edge can be calculated with the aid of the appropriate value of the surface pressure gradient. Similarly, the flow conditions at an initial point on the shock wave can be obtained with the aid of the corresponding value of the shock-wave curvature. Additional points can be obtained between these two by linear interpolation. If the two initial points are chosen as the ends of a first-family Mach line, there is sufficient information available to determine the curvature of this Mach line. Therefore, if detailed knowledge of the flow in the region of the leading edge is required, the surface, shock wave, and first-family Mach line can be approximated by circular arcs. (See ref. 17.)

INVESTIGATION OF THE FLOW ABOUT AIRFOILS AND DISCUSSION OF RESULTS

This study is divided into two sections: first, an investigation of the flow in the region of the leading edge of curved airfoils; and second, an investigation of the complete flow field about an example airfoil. Each of these sections is further subdivided into a consideration of the effects of Mach number, assuming air behaves as an ideal gas, and into a consideration of the combined effects of Mach number and gaseous imperfections. In the latter regard, the principal emphasis is placed on the caloric imperfections previously discussed.

FLOW IN THE REGION OF THE LEADING EDGE OF CURVED AIRFOILS

Ideal-gas flow.—The results of the calculations (using eq. (D4)) of the surface pressure gradient are presented in table II and figure 2.[7] The values presented in the table are for a range of Mach numbers from 1.5 to ∞ and for leading-edge deflection angles from 0° to 45°. Where no value appears in the table, the flow behind the shock wave is subsonic. Corresponding results of the calculations of surface-pressure-gradient ratio are presented in table III and figure 3. From these results it is seen that except near shock detachment, the surface-pressure-gradient ratio varies only from 0.98 to 1.02 for Mach numbers less than 4. Therefore, very little error will result from the use of the shock-expansion method for the surface pressure gradient at these lower Mach numbers. For Mach numbers greater than 4 (even

[7] Charts were also presented for surface pressure gradient, surface-pressure-gradient ratio, and shock-wave curvature for ideal-gas flows in reference 9; however, the results given in the present report are somewhat more extensive. These results were also presented in cross-plotted forms in reference 17.

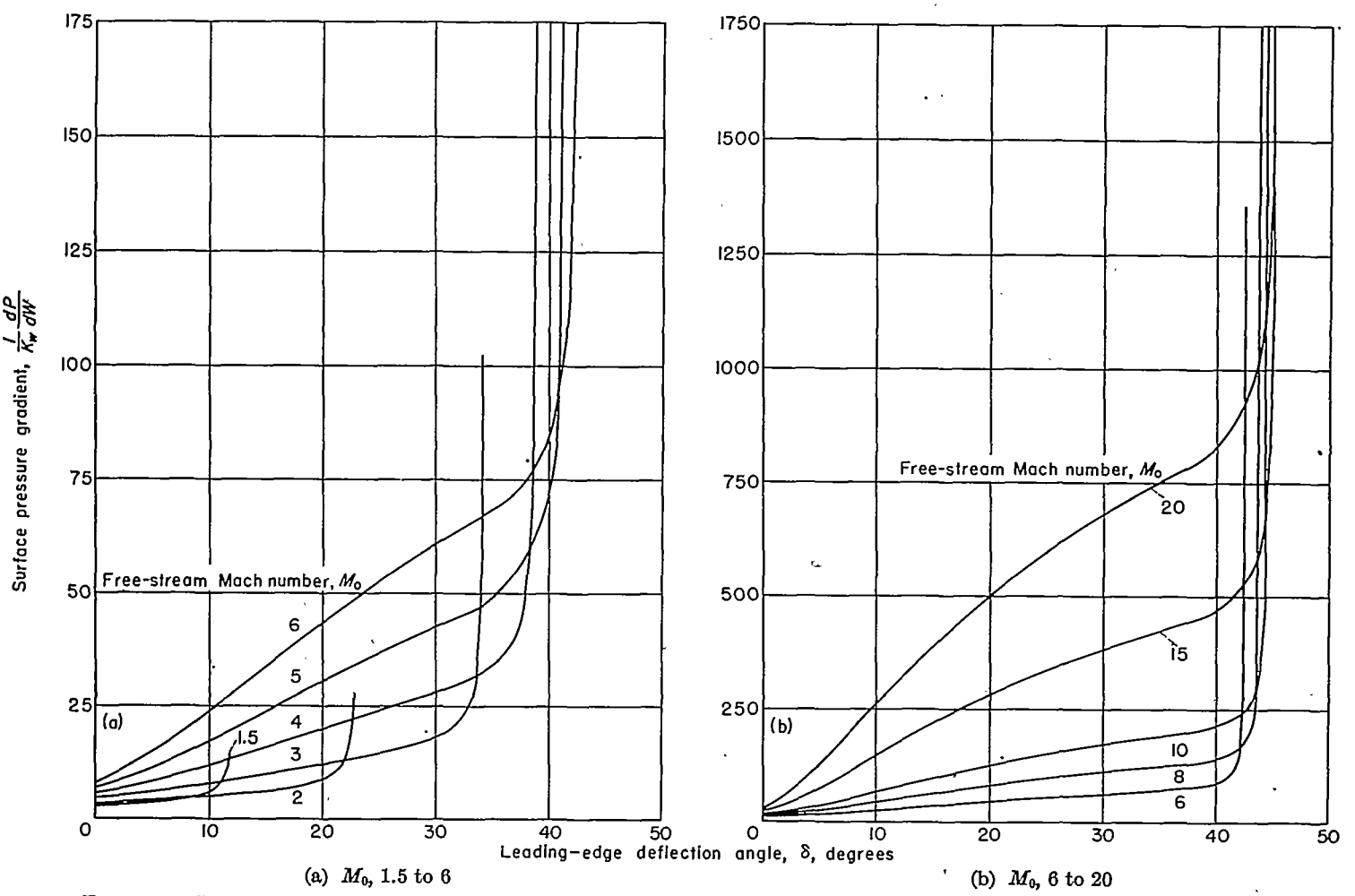

(a) M_0, 1.5 to 6 (b) M_0, 6 to 20

FIGURE 2.—Variation of surface pressure gradient with leading-edge deflection angles for various free-stream Mach numbers.

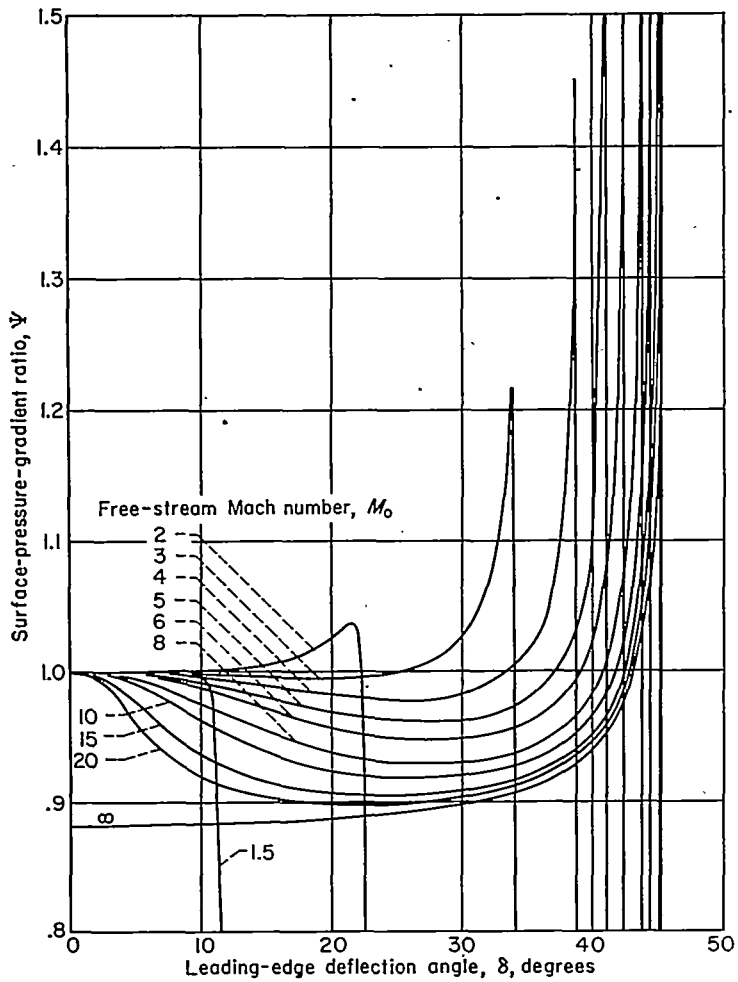

FIGURE 3.—Variation of surface-pressure-gradient ratio with deflection angle for various free-stream Mach numbers.

including ∞),[8] the ratio only varies between about 0.9 and 1.1 (again except near detachment) and, therefore, only small error might be expected from the use of the shock-expansion method. Near detachment, at the higher Mach numbers, the surface-pressure-gradient ratio attains a very large range of values and the maximum value increases with Mach number. For these conditions, then, the use of the shock-expansion method for calculating the surface pressure gradient at the leading edge would result in appreciable error.

The flow along the surface is isentropic. Hence, it can be shown that ψ, the ratio of surface pressure gradient to that given by the generalized shock-expansion method, is also the velocity-gradient ratio, the Mach number gradient ratio, the Mach angle gradient ratio, the density-gradient ratio, and the temperature-gradient ratio. Any of these gradients may be found, then, by calculating the gradient, using the shock-expansion method and applying the appropriate value of ψ. This property of the ratio ψ makes it useful in the application of the method of characteristics with any of the coordinate systems commonly employed in the compatibility equations.

The results of the calculations of shock-wave curvature (eq. (D5)) are presented in table IV and figure 4.[9] Similarly, the results of the calculations of shock-wave-curvature ratio (eq. (44)) are presented in table V and figure 5. Except near detachment, the curvature ratio varies from 0.92 to 1.08 for all Mach numbers including ∞.[10] Thus, only small errors would result from using the value of the shock-wave curvature given by the shock-expansion method for all flow conditions except near shock detachment.

Calorically-imperfect-gas flows.—With increasing Mach number and leading-edge slope, the temperature ratio across an oblique shock wave increases as shown in figure 6. As the temperature behind the shock wave increases, the behavior of air diverges from that of an ideal gas as discussed previously. Below 800° R., the divergence is not significant, and the equations for ideal-gas flow can be applied with only minute errors resulting. Above 800° R., the energy of the vibrational degrees of freedom of the gas molecules is appreciable and becomes greater with increasing temperature. For these conditions, the specific heats and their ratio vary significantly with temperature. The equations developed previously consider these effects and permit the extension of the solution for surface pressure gradient and shock-wave curvature to the case of calorically imperfect gases. These

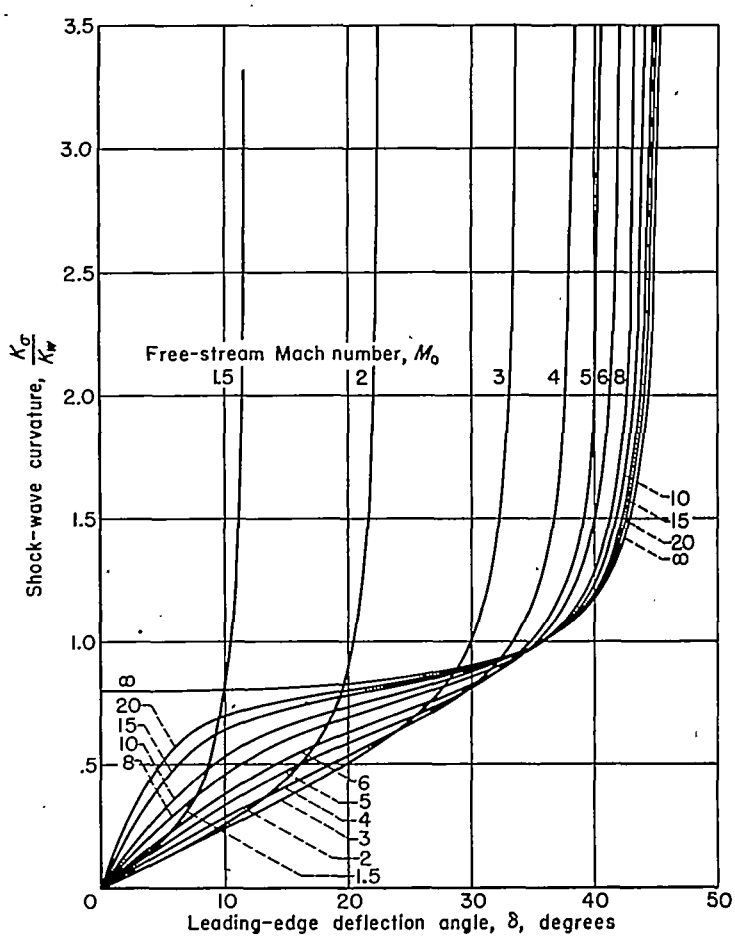

FIGURE 4.—Variation of shock-wave curvature with leading-edge deflection angle for various free-stream Mach numbers.

[8] For the particular case of infinite free-stream Mach number and zero deflection angle, the pressure-gradient ratio is double valued. From equation (D6), it is apparent that ψ is unity or zero deflection. Yet, at infinite Mach number, ψ approaches $\frac{3}{2\gamma-1}\sqrt{\frac{\gamma(\gamma-1)}{2}}$ as the deflection angle approaches zero.

[9] As in the case of ψ, K_σ/K_∞ has the double values of 0 and $\frac{(\gamma+1)^3}{4(2\gamma-1)}$ for $M_0=\infty$, $\delta=0$.

[10] As in the case of ψ and $K_\sigma/K_{\infty,\varepsilon}$ has the double values of 1 and $\frac{\gamma+1}{2(2\gamma-1)[1-\sqrt{(\gamma-1)/2\gamma}]}$ for $M_0=\infty$, $\delta=0$.

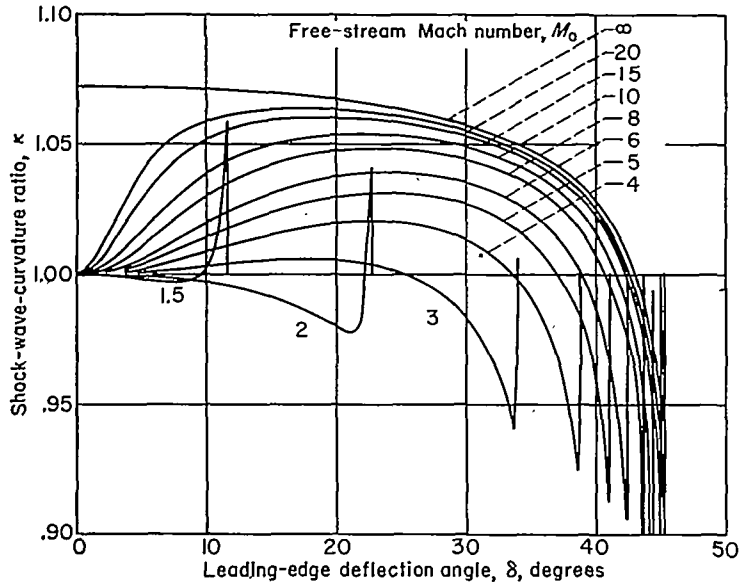

FIGURE 5.—Variation of shock-wave-curvature ratio with leading-edge deflection angle for various free-stream Mach numbers.

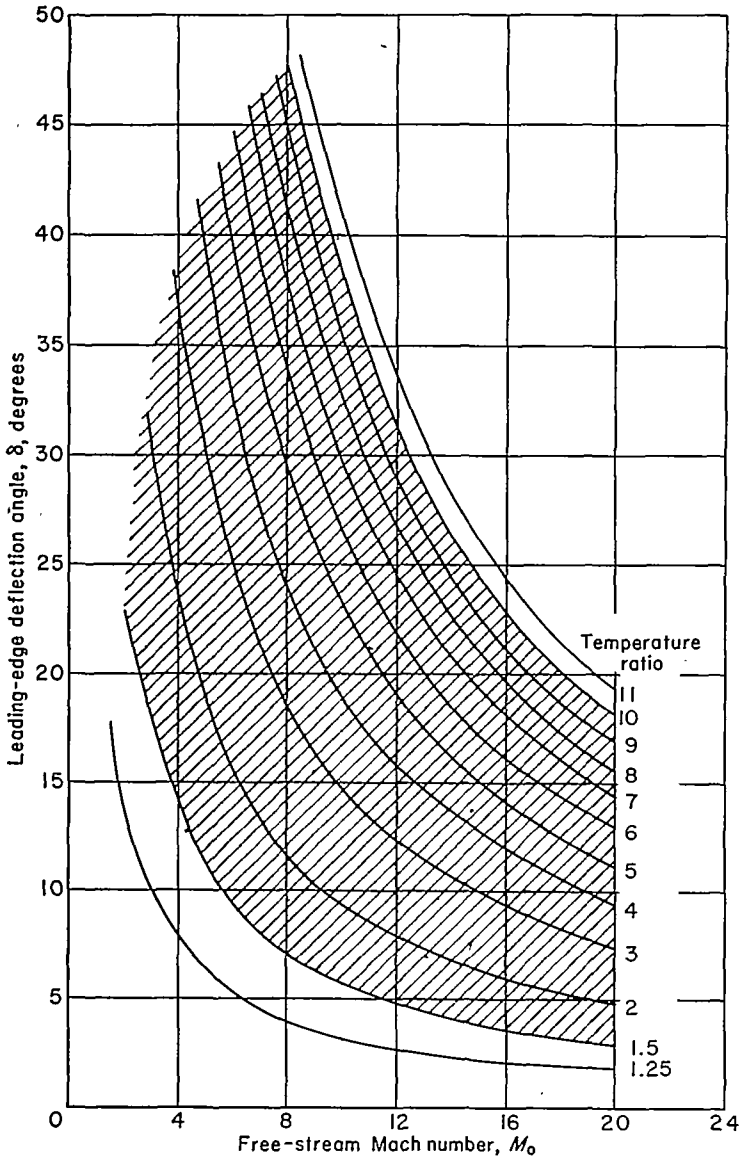

FIGURE 6.—Variation of leading-edge deflection angle with free-stream Mach number for various values of the temperature ratio.

equations are valid for temperatures up to the order of 5,000° R. For a free-stream temperature of 500° R., therefore, the shaded area between lines of constant temperature ratio of 1.5 and 10, in figure 6, represents the range of conditions for which the method developed in this report for the flow of a diatomic, calorically imperfect gas would apply.

The excitation of the vibrational degrees of freedom of the gas molecules requires a finite number of collisions, causing the well-known heat-capacity lag discussed in references 5 and 6. The flow distance (i. e., along the streamline) required to establish equilibrium is usually small in dense air and will be considered infinitesimal in this report. Also, the dissociation of air (see ref. 6) will not be considered here.

Since the free-stream static temperature is an additional parameter in calculations of flow of imperfect gases, only a limited number of calculations of $(1/K_w)\ (dP/dW)$, ψ, K_σ/K_w, and κ were made. The purpose of these calculations is to compare the variations of these quantities with the values as given by the ideal-gas-flow computations. The calculations followed the procedure described in Appendix D. A free-stream static temperature of 500° R. was used. The results of these calculations are presented in table VI for various Mach numbers and leading-edge deflection angles.

The surface pressure gradients for an ideal gas and for a calorically imperfect, diatomic gas are compared in figure 7. In all cases calculated, the gradient is smaller for the imperfect gas and diverges gradually, with increasing free-stream Mach number and deflection angle, from the value of the gradient for an ideal gas. This divergence is consistent with the increasing effects of the caloric imperfections due to the increasing temperature behind the shock wave.

The surface-pressure-gradient ratio for the imperfect gas is compared in figure 8 with the ratio for an ideal gas. The surface-pressure-gradient ratio is smaller for imperfect-gas flows than for ideal-gas flows indicating that the effects of shock-wave and expansion-wave interaction are greater. This result is attributed, in part, to the fact that the angle between the shock wave and the airfoil surface is smaller for

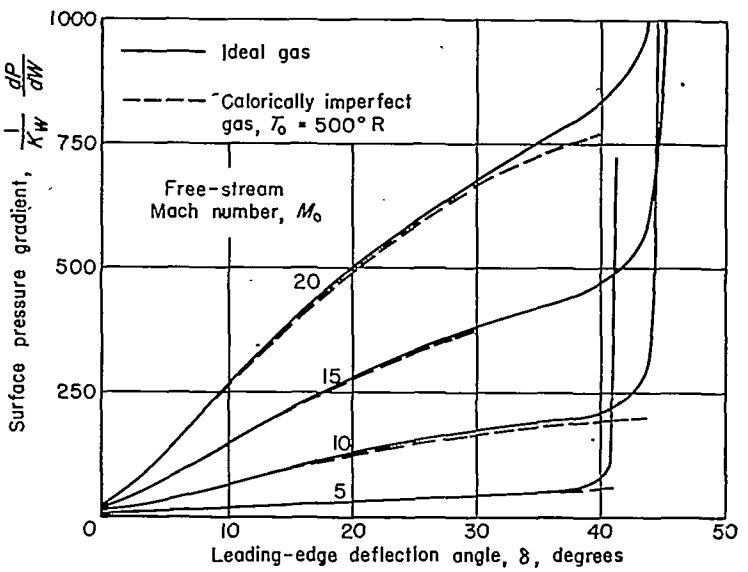

FIGURE 7.—Comparison of the variation of surface pressure gradient with leading-edge deflection angle for various free-stream Mach numbers for an ideal gas and for a calorically imperfect, diatomic gas.

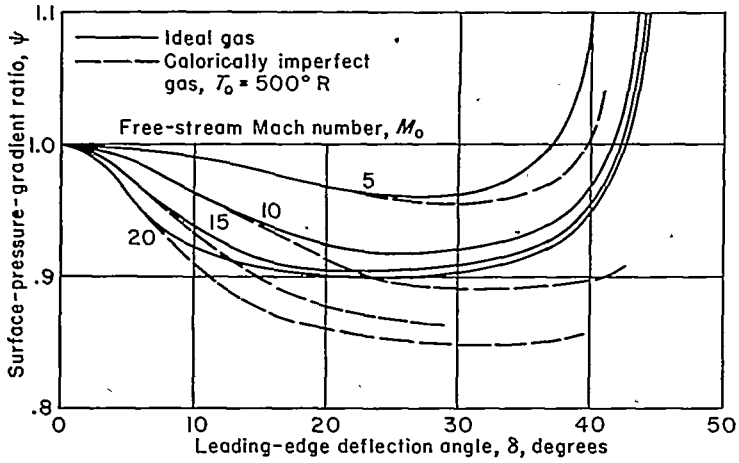

FIGURE 8.—Comparison of the variation of surface-pressure-gradient ratio with leading-edge deflection angle for various free-stream Mach numbers for an ideal gas and for a calorically imperfect, diatomic gas.

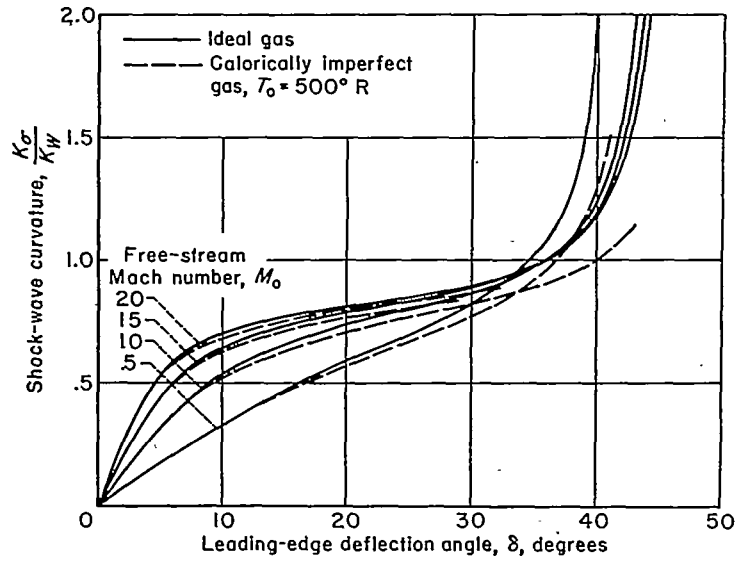

FIGURE 9.—Comparison of the variation of the shock-wave curvature with the leading-edge deflection angle for various free-stream Mach numbers for an ideal gas and for a calorically imperfect, diatomic gas.

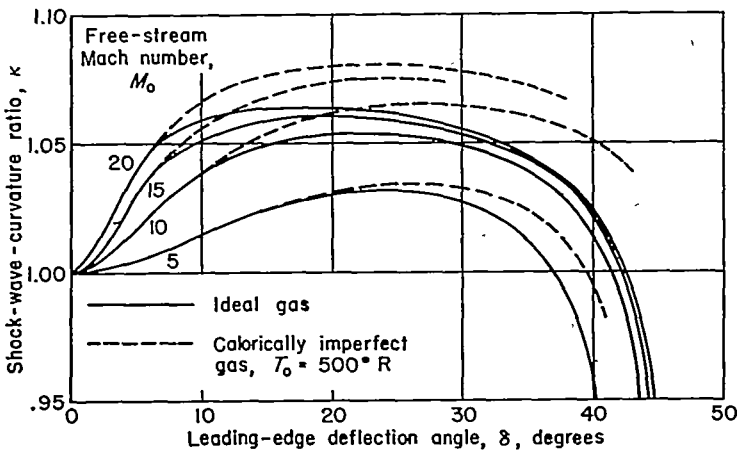

FIGURE 10.—Comparison of the variation of shock-wave-curvature ratio with leading-edge deflection angle for various free-stream Mach numbers for an ideal gas and for a calorically imperfect, diatomic gas.

imperfect-gas flows than for ideal-gas flows. The difference between the imperfect- and ideal-gas calculations increases with increasing Mach number and deflection angle, as might be expected. In the range of Mach numbers and flow deflection angles investigated, however, the extreme values of ψ differ only by about 5 percent (see fig. 8). Thus, it is apparent that while the shock-expansion method will not be quite as accurate for calorically-imperfect-gas flows as for ideal-gas flows, the method will not be expected to be invalidated.

A divergence with Mach number and deflection angle is also apparent in figure 9 in which the shock-wave curvatures for an ideal gas and a calorically imperfect, diatomic gas are compared. This divergence is compatible with the change in surface pressure gradient due to the caloric imperfections of the gas. The shock-wave-curvature ratio for a calorically imperfect, diatomic gas and this ratio for an ideal gas are shown in figure 10. Again, it is seen that the effect of caloric imperfection is to increase the effects of shock-wave and expansion-wave interaction.

COMPLETE FLOW FIELDS

Ideal-gas flows.—The effects of Mach number of primary interest here are, of course, those which result from the interaction between the leading-edge (or other) shock wave and small disturbances originating on the surface of an airfoil. Although the reflected disturbances that are the product of this interaction will have the largest effect on the flow near the leading edge, their influence on the complete flow field about an airfoil also warrants investigation. Further insight into these effects can be obtained in the region just downstream of the shock wave without regard for the shape of the airfoil producing the shock. To this end, it is convenient to consider the ratio $\frac{\partial\delta/\partial C_1}{\partial\delta/\partial C_2}=-\frac{\partial p/\partial C_1}{\partial p/\partial C_2}$ (see eq. (25)) which may be termed "the disturbance strength ratio" since, in the region under consideration, it is a measure of the ratio of strengths of disturbances reflected from the shock wave to disturbances incident on the wave. This ratio may be evaluated with equation (40). This calculation has been carried out for Mach numbers from 3.5 to ∞ (γ=1.4) and flow deflection angles approaching those corresponding to shock detachment (i. e., $M_\sigma \approx 1$), and the results are presented in figure 11. It is evident that except near M_σ=1,

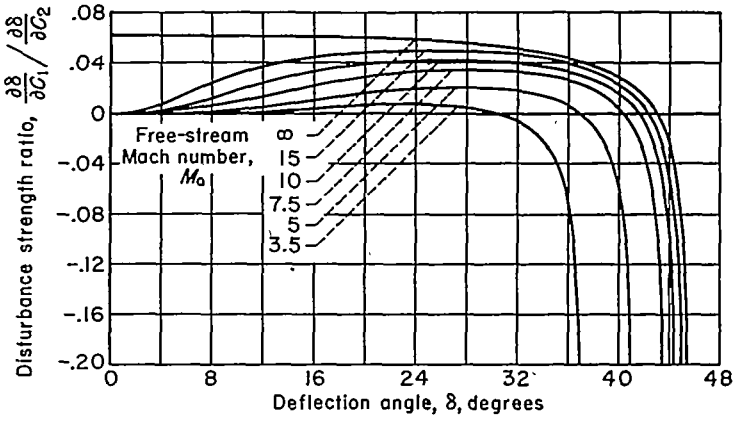

FIGURE 11.—Variation with deflection angle of the disturbance strength ratio behind an oblique shock wave for various free-stream Mach numbers (γ=1.4).

the ratio is small (in absolute value) compared to 1 throughout the entire range considered—this observation also applies, of course, at lower supersonic Mach numbers. Thus it is indicated that almost all of an incident disturbance is generally absorbed in the shock wave, provided the air behaves like an ideal diatomic gas. This result is substantially the same, of course, as that which is assumed in deriving the shock-expansion method of calculating flows about airfoils, and therefore yields additional credence in the method for high Mach number as well as low Mach number applications. It should also be noted that this result is contrary to that obtained by Lighthill (ref. 18), who reports that for hypersonic flows($M_0\,\delta \gg 1$) a disturbance is reflected from a shock wave with opposite sign but essentially undiminished strength. Lighthill's conclusion is based on an incorrect evaluation of his results for the case of very high Mach numbers.

As an over-all check on the shock-expansion method, surface pressure distributions calculated thereby are compared in figure 12 with those obtained with the method of characteristics for a 10-percent-thick parabolic-arc biconvex airfoil ($\alpha=0°$) operating at free-stream Mach numbers of 3.5, 10, and ∞. (Additional calculations presented in ref. 19 were also performed for $M_0=5$, 7.5, and 15.) Predictions of the slender-airfoil approximation to the former method for high supersonic speeds are also shown. There is no apparent difference between the pressure distributions given by the method of characteristics and the shock-expansion method at a Mach number of 3.5; at a Mach number of 10, and more so at infinite Mach number, however, the latter method predicts pressures which are slightly low downstream of the nose. This result would be deduced from figure 11 where it is observed that, at the Mach numbers under consideration, expansion waves incident on the nose shock wave are reflected back toward the surface as compression waves of relatively small but increasing strength with increasing Mach number. The effect of these waves does not become pronounced even at infinite Mach number (see fig. 12 (c)) and it can be seen, upon comparison of these results with those presented previously for the pressure-gradient ratio (see fig. 3) that the effect of the reflected waves dissipates somewhat downstream of the nose. The shock-expansion method is thus further substantiated as being a reliable simplified method for predicting the flow about airfoils at high supersonic speeds, again, so long as the air behaves as an ideal diatomic gas. The further simplified slender-airfoil method also appears to be a good approximation over the entire range of Mach numbers,[11] although, as would be expected from the assumptions made in its development, it is in somewhat greater error than the shock-expansion method at lower Mach numbers.

The shape of the shock wave given by the shock-expansion method, as presented in Appendix B, is compared in figure 13 with the shape given by the method of characteristics for the biconvex airfoil at $M_0=\infty$. (These shock waves correspond to the pressure distributions given in fig. 12 (c).) The shock-expansion method gives a reasonably good approximation to the shock-wave shape though, as would be expected from the results given in figure 5, the curvature is somewhat too small. (A procedure for getting a closer approximation to the shock-wave shape is also given in Appendix B.) It can be seen, however, that this method of determining the shock-wave shape is far better than the assumption of a straight shock wave that is often associated with the shock-expansion method. Evidently, then, the shock-expansion method can also be used to calculate the flow in regions away from the airfoil surface. (See Appendix B.)

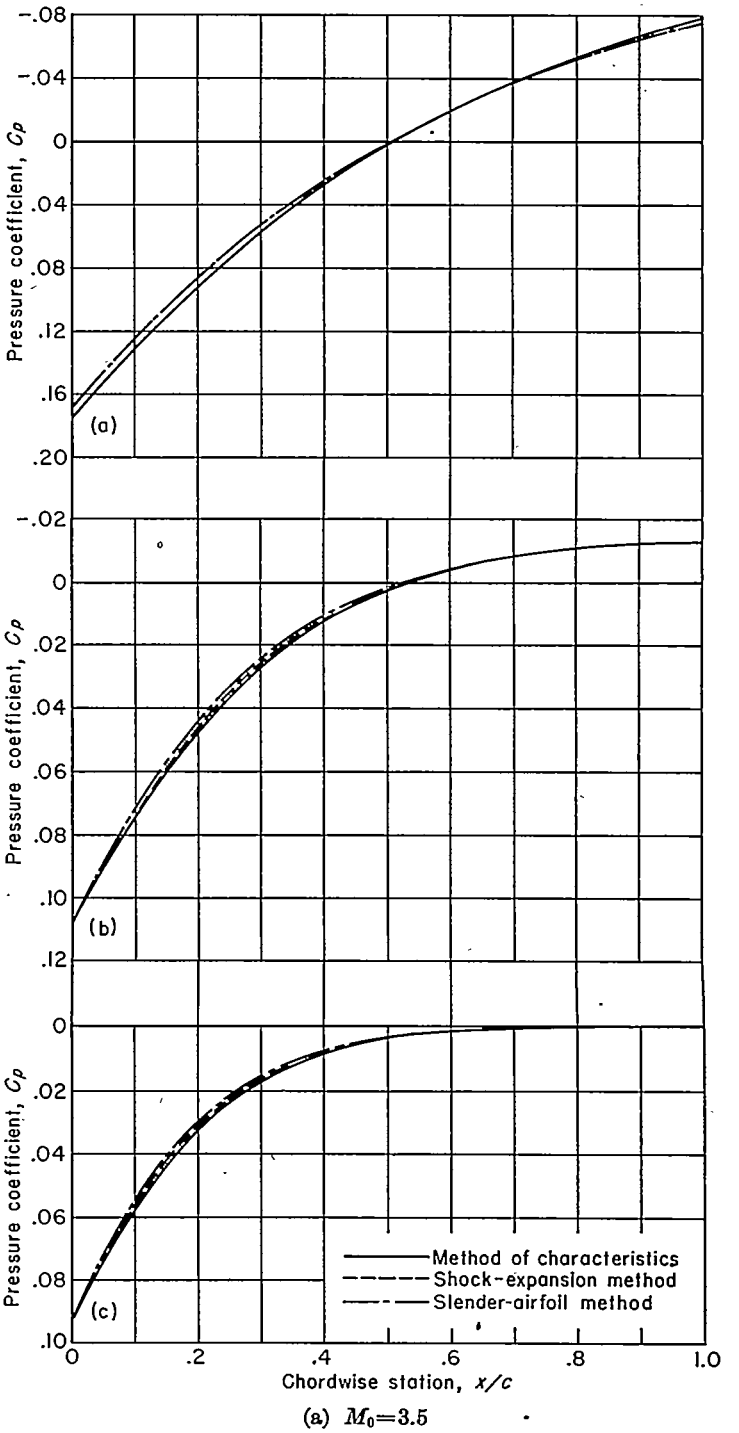

(a) $M_0=3.5$
(b) $M_0=10$
(c) $M_0=\infty$

FIGURE 12.—Pressure distribution on 10-percent-thick biconvex airfoil section for various free-stream Mach numbers at $\alpha=0°$.

[11] The hybrid expression for pressure coefficient obtained by Ivey and Cline (ref. 5) gives reasonably good results also, although not as accurate as the slender-airfoil method at the higher Mach numbers under consideration.

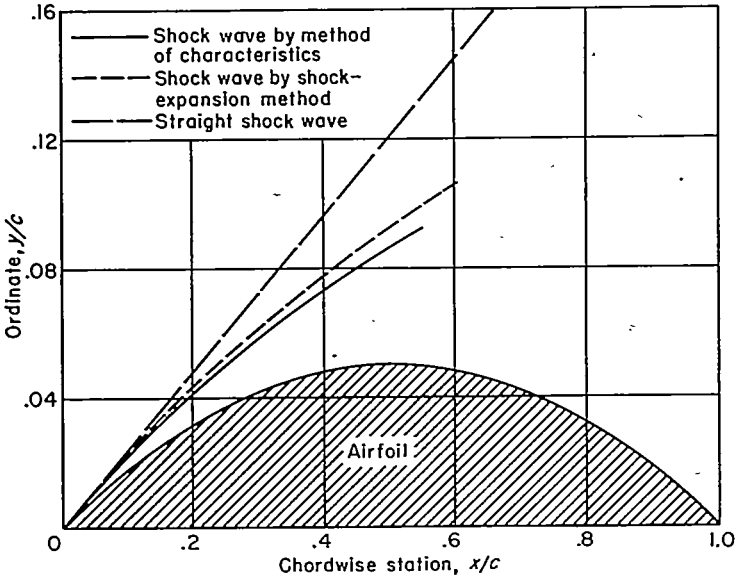

FIGURE 13.—Shape of the shock wave for 10-percent-thick biconvex airfoil section at $\alpha=0°$ and $M_0=\infty$.

The relative accuracy at high Mach numbers of the slender-airfoil method and linear and second-order potential theories may be seen in figure 14. As might be expected, the slender-airfoil method is more accurate than linear theory at both $M_0=5$ and 15 and more accurate than second-order theory at $M_0=15$. It is perhaps surprising to note, however, that at the lower Mach number of 5, the slender-airfoil method is also somewhat superior to the second-order theory.

The pressure distributions of figures 12 and 14 have been employed to calculate the zero-lift drag of the biconvex airfoil, and the results of these calculations, along with additional predictions of the different methods, are shown in figure 15. Predictions of the shock-expansion method are, of course, in best agreement with those of the method of characteristics; while the slender-airfoil method, although slightly less accurate than the shock-expansion method, is apparently superior to both linear and second-order theories at Mach numbers above 3.5.

The preceding findings verify that, so long as the disturbance strength ratio is small compared to 1, the flow along streamlines is essentially of the Prandtl-Meyer type. If we choose, on the basis of these findings, a maximum absolute value for $\frac{\partial\delta/\partial C_l}{\partial\delta/\partial C_d}$ of 0.06 (note the maximum value of $\frac{\partial\delta/\partial C_l}{\partial\delta/\partial C_d}$ for the cases presented in fig. 12 was approximately 0.06 at $M_0=\infty$), the region in which the shock-expansion method is applicable can readily be obtained from figure 11. The upper boundary line of this region is shown in figure 16, and it is evident that it lies only slightly below (about 1°, in general) the line corresponding to shock detachment given approximately by the $M_s=1.0$ line. Almost the entire region of completely supersonic (ideal gas) flow is then covered by the method. (See shaded area of fig. 16.) The range of applicability shown in figure 16 is appreciably larger than that indicated by Rand (ref. 20) who required

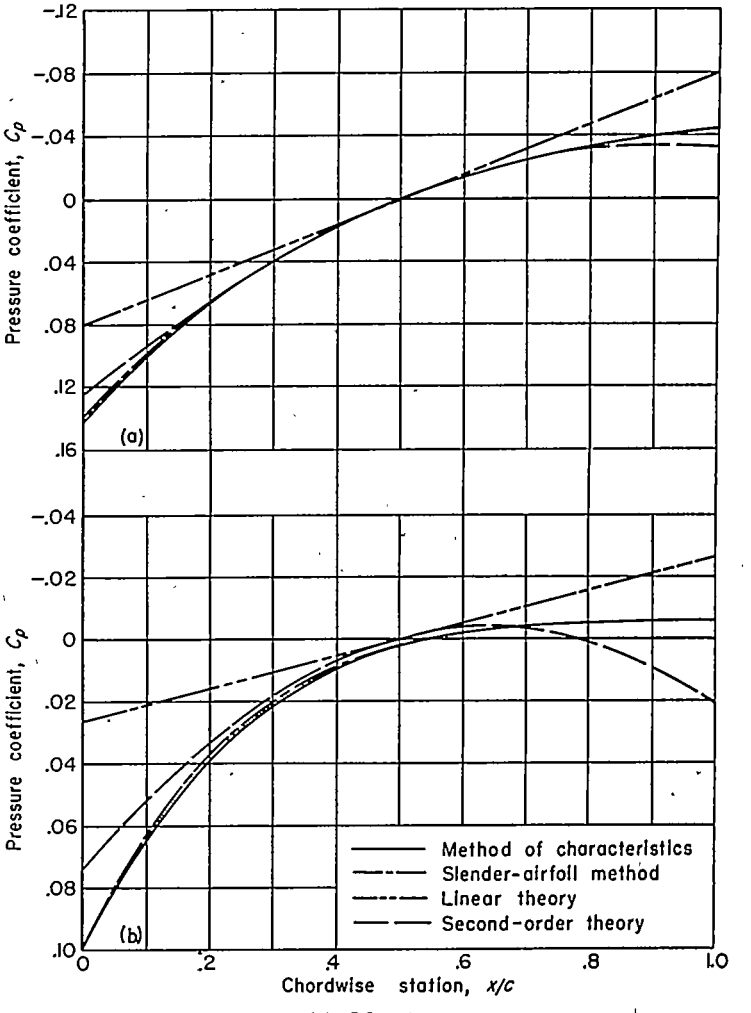

(a) $M_0=5$
(b) $M_0=15$

FIGURE 14.—Pressure distribution on 10-percent-thick biconvex airfoil section at $\alpha=0°$.

that the entire flow field be of the true Prandtl-Meyer type (i. e., that all flow properties be constant along first-family Mach lines and not just δ and p). The results presented in

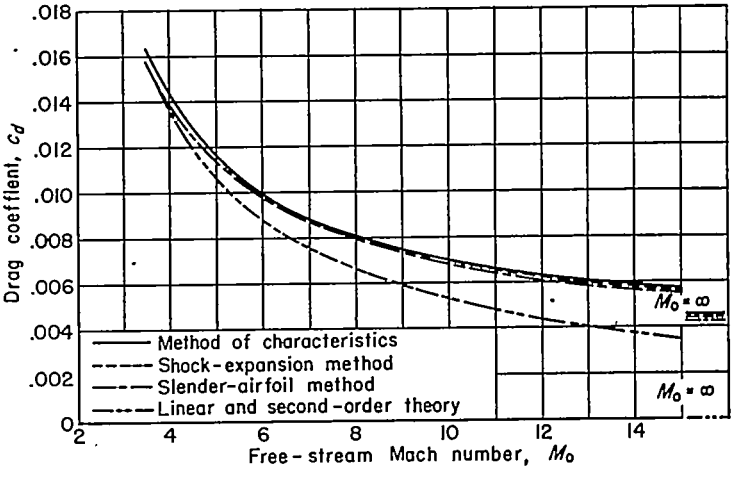

FIGURE 15.—Variation of drag coefficient with free-stream Mach number for 10-percent-thick biconvex airfoil section at $\alpha=0°$ ($\gamma=1.4$).

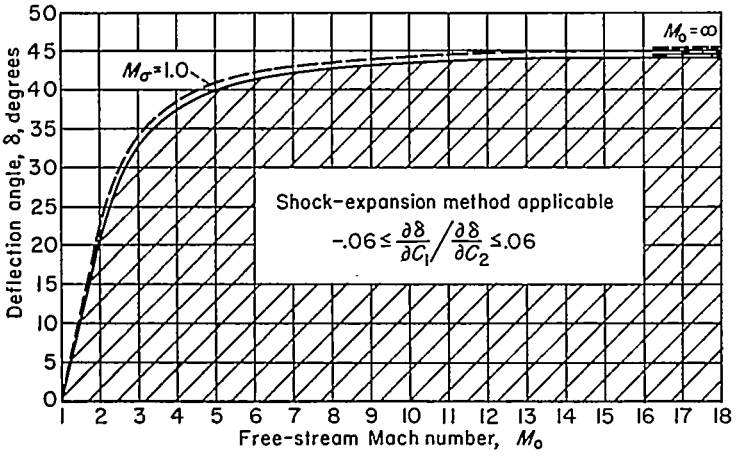

FIGURE 16.—Range of applicability of shock-expansion method ($\gamma=1.4$).

figures 12 and 13 show, however, that this restriction is not necessary.

The question naturally arises concerning the corresponding range of applicability of the slender-airfoil method. This question may be answered, in part, by comparing separately the predictions of the method for oblique-shock flows and expansion flows with those of the exact oblique-shock equations and Prandtl-Meyer equations. Such a comparison is shown in figure 17 in terms of the percentage

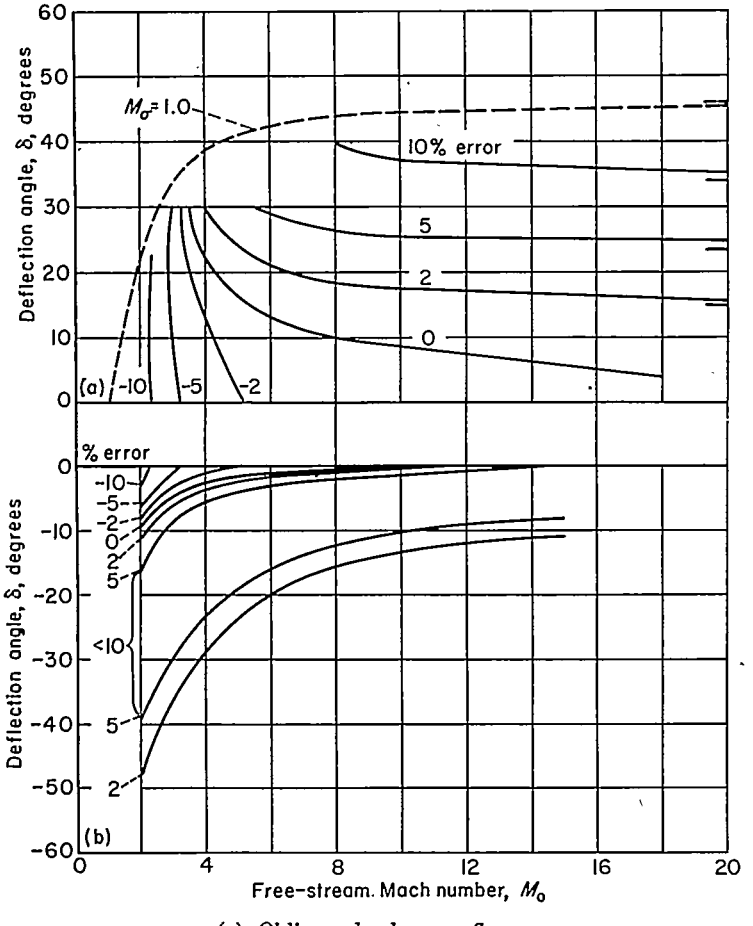

(a) Oblique-shock-wave flows.
(b) Expansion flows.

FIGURE 17.—Accuracy of slender-airfoil method in predicting pressure coefficients ($\gamma=1.4$).

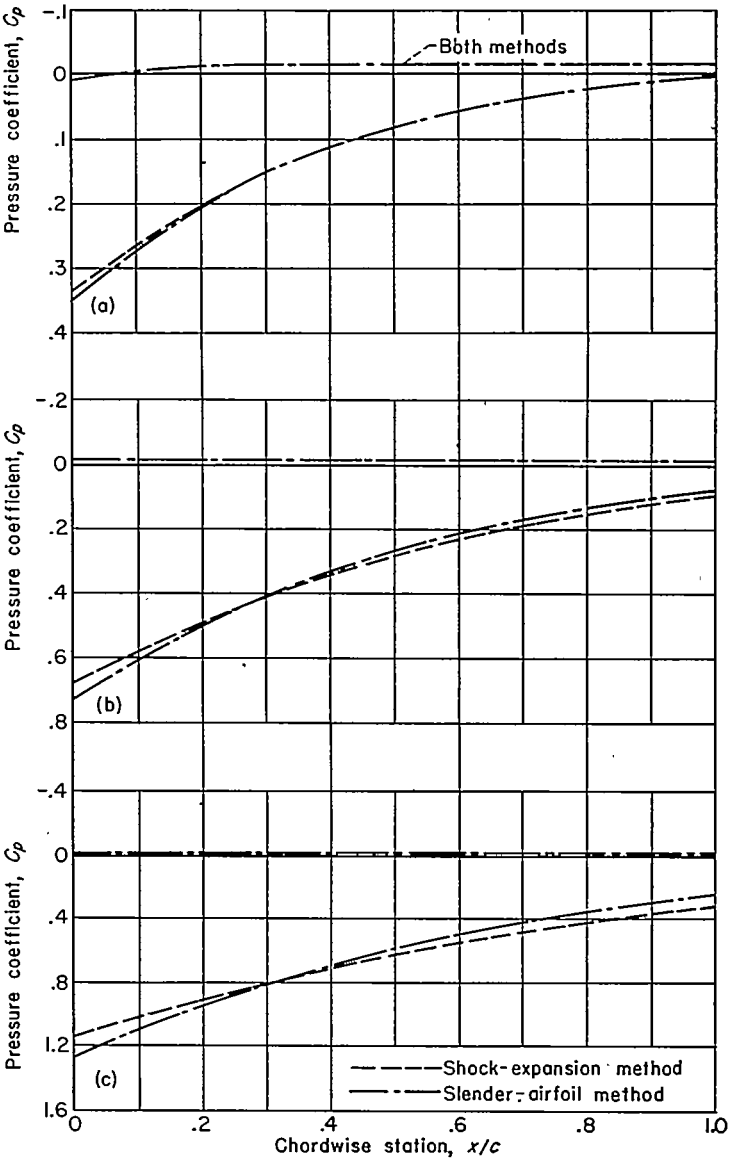

(a) $\alpha=10.0°$
(b) $\alpha=19.9°$
(c) $\alpha=30.0°$

FIGURE 18.—Pressure distribution on 10-percent-thick biconvex airfoil section for various angles of attack at $M_0=10$ ($\gamma=1.4$).

error in the pressure coefficients predicted by the slender-airfoil method. As would be expected, this method does not exhibit good accuracy over the wide range of applicability of the shock-expansion method; however, it is indicated that it should predict pressure coefficients with less than 10-percent error down to Mach numbers as low as 3 for airfoils producing flow deflections up to as high as 25°.

As a further check on the utility of the slender-airfoil method, the pressure coefficients on the 10-percent-thick biconvex airfoil have been calculated with this method and the shock-expansion method at a Mach number of 10 and angles of attack up to about 30°.[12] The results of this calculation are shown in figure 18 (see fig. 12 (b) for $\alpha=0°$)

[12] These conditions are within the range of applicability of the shock-expansion method as defined in figure 16; hence, the use of the method as a base of comparison seems justified. Since the shock-expansion method is far less tedious to apply than the method of characteristics, it will be employed as such a base in subsequent calculations whenever the conditions being investigated have been determined to be within its range of applicability.

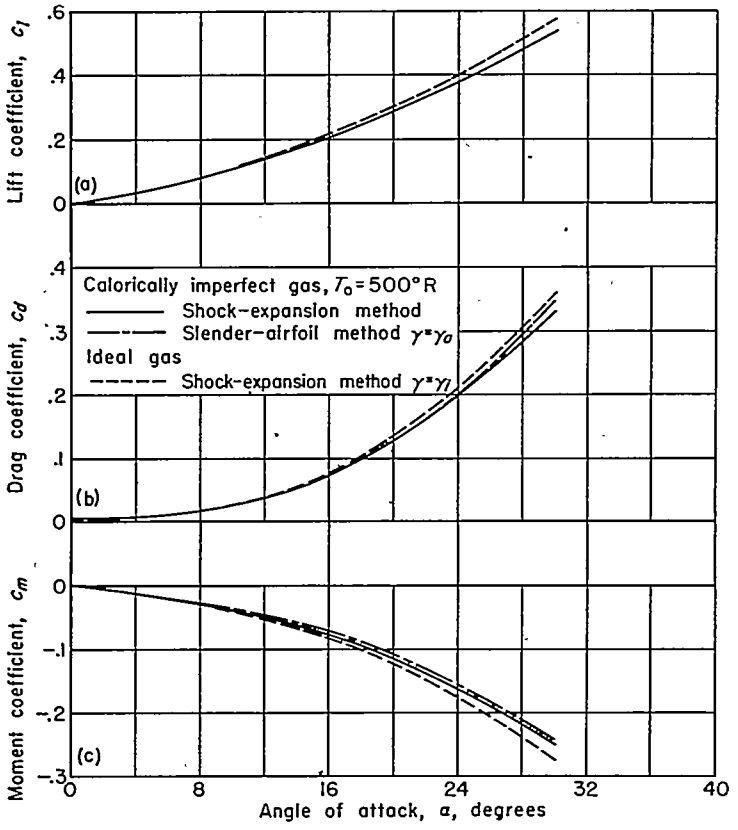

(a) Lift coefficient.
(b) Drag coefficient.
(c) Moment coefficient.

FIGURE 19.—Variation of force and moment coefficients with angle of attack for 10-percent-thick biconvex airfoil section at M_0=10 (γ=1.4).

where it is seen that the agreement is reasonably good, even at the highest angle of attack. This fact is reflected in figure 19 showing the force and moment coefficients for the airfoil as a function of angle of attack. Little difference is observed in the force coefficients as calculated by the two methods, while the moment coefficients display more pronounced but, nevertheless, small differences at the higher angles of attack.

From these and previous considerations, the ranges of applicability of the shock-expansion and slender-airfoil methods for supersonic ideal-gas flows are reasonably well established. It remains now to determine the manner and extent to which gaseous imperfections in the flow at higher supersonic speeds may alter these ranges, and the reasons therefor.

Imperfect-gas flows.—As a first step toward investigating the effects of gaseous imperfections on the high Mach number flows under consideration, it is convenient to extend our consideration of the disturbance strength ratio $\frac{\partial\delta/\partial C_l}{\partial\delta/\partial C_d}$. It is recalled that when air exhibits a constant value of γ equal to 1.4 (the value for an ideal diatomic gas), the disturbance strength ratio is small at arbitrarily large Mach numbers, provided the flow deflection angles are not too close to those for shock detachment. One of the most important effects of gaseous imperfections is, however, to decrease γ of the disturbed air below this value due to the excitation of additional degrees of freedom (e. g., vibrational) in the molecules at the high temperatures encountered at high Mach numbers. Indeed, at arbitrarily high Mach numbers it might be expected that γ of the disturbed air would approach 1, since the number of degrees of freedom may effectively become very large (see, e. g., refs. 3 and 6). In this case, however, the extent of the disturbance flow field is decreased to a layer at the surface of the body which is negligibly thin compared to that for the case of ideal-gas flow. Thus, it is apparent that significant changes in the flow about airfoils at high Mach numbers may result from decreases in γ of the disturbed air; hence, the effects of such decreases on the disturbance strength ratio would appear to warrant attention.

A detailed analysis of these effects is impractical at the present time, due to the limited range over which the variation of γ with temperature is accurately known. Even in the range where this variation is so known, the additional complication required to consider the effects of variable γ and the addition of another independent parameter (free-stream temperature) make extensive calculations of the disturbance strength ratio impractical. However, some knowledge of these effects can be gained by performing the calculations for one free-stream Mach number and temperature. Such calculations have been carried out at a Mach number of 10 for a free-stream temperature of 500° R. and the results are presented in figure 20. The curve for a calorically imperfect gas cannot be extended to shock detachment because the temperature behind the shock wave exceeds that for which the calorically-imperfect-gas equations are valid. It can be seen that the effect of the caloric imperfection of air is to increase the value of the disturbance strength ratio and that the effect increases with increasing temperature or decreasing γ. However, it appears that if γ does not decrease appreciably below 1.3, as in this case, the disturbance strength ratio is still small compared to unity. It might be expected, therefore (as previously found for flow in the region of the leading edge), that the shock-expansion method would continue to predict the flow about complete airfoils with reasonable accuracy. This point has been checked with the methods developed previously for analyzing the flow of a calorically imperfect, diatomic gas at local air temperatures up to about 5,000° R. (note γ has a value only

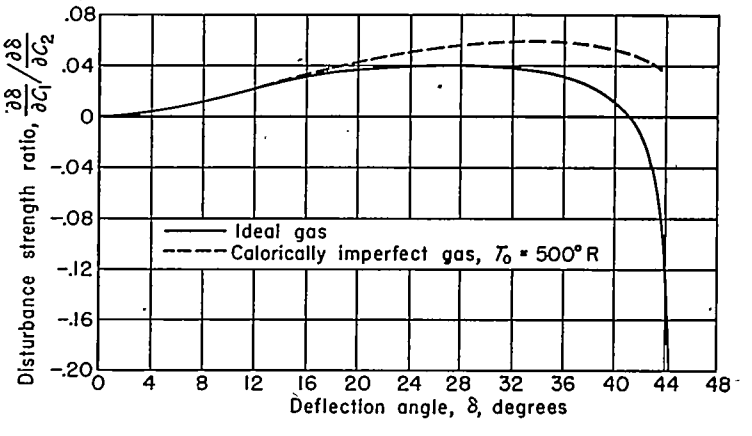

FIGURE 20.—Effect of the caloric imperfections of air on the disturbance strength ratio at M_0=10 and T_0=500° R.

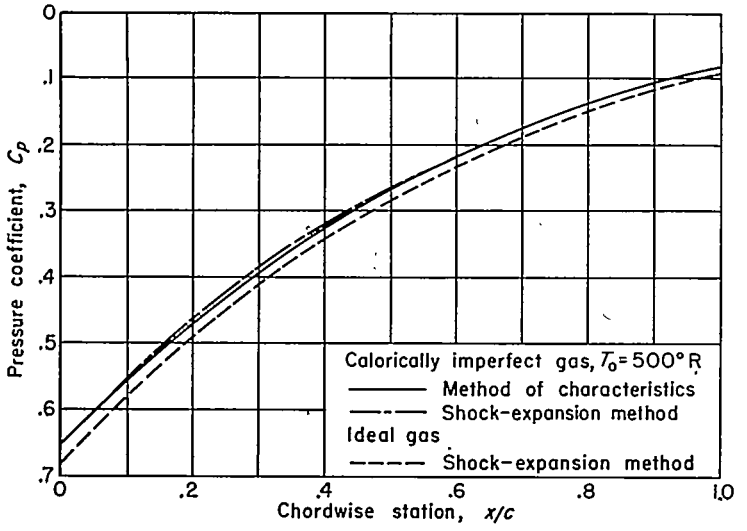

FIGURE 21.—Pressure distribution on lower surface of 10-percent-thick biconvex airfoil section at $M_0=10$, $T_0=500°$ R, $\alpha=19.9°$.

slightly less than 1.3 at this temperature). In particular, the pressure distribution on the lower surface of the biconvex airfoil at $M_0=10$, $\alpha=19.9°$, and $T_0=500°$ R. ($T_N \approx 4000°$ R.) has been calculated with both the method of characteristics and the shock-expansion method.[13] The results of these calculations are presented in figure 21, and it would appear that the conclusions drawn from figure 20 are substantiated. (Due to the lower temperatures, pressures in the expansion flow about the upper surface are not influenced by caloric imperfections and, hence, are the same as shown in figure 18 (b).) For these same conditions, the shapes of the shock waves given by the shock-expansion method and by the method of characteristics (both for a calorically imperfect gas) are compared in figure 22. Just as in the case of ideal-gas flows, the shock-expansion method gives a good approximation to the shock-wave shape, far better than the assumption of a straight shock wave. Thus, it is seen that the conclusion drawn from figure 20 should also apply for the use of the shock-expansion method to calculate the flow field away from the airfoil surface.

Shown also in figure 21 is the pressure distribution obtained by the shock-expansion method for an ideal gas ($\gamma_i=1.4$). It is apparent, on comparing this pressure distribution with the other distributions, that although the effect of caloric imperfections on the disturbance strength ratio is small, the pressures are appreciably reduced by the increase in specific heats. The extent of this reduction is more completely illustrated in figure 23 where the lower-surface pressure distributions on the biconvex airfoil are presented for $M_0=10$ and $T_0=500°$ R., at $\alpha=0°$, 10°, 19.9°, and 30°. As one might expect, the reduction in pressures increases with angle of attack (due to the corresponding increase in static temperature of the disturbed air). The pressure coefficients calculated with consideration of the imperfections in the gas are less on the lower surface (up to 6 percent at the leading edge and 15 percent at the trailing edge) than those calculated assuming the gas behaves ideally. The upper-surface pressures are again unaffected by the caloric imperfections of air in all the cases presented (except at $\alpha=0°$) since this surface experiences lower pressures and, hence, lower temperatures. They are therefore the same as shown in figure 18. Shown also in figure 23 are the pressure distributions calculated with the slender-airfoil method for $\gamma=\gamma_a$. The accuracy of this simplified method is substantially the same as was previously observed for the corresponding method in the case of ideal-gas flows, although the local error may be greater than the reduction in pressure coefficients due to the caloric imperfections of air.

The force and moment coefficients, corresponding to the lower-surface pressure distributions shown in figure 23 and the upper-surface distributions of figure 18, are presented in figure 24. The reduction in the lower-surface pressures leads, of course, to a general reduction in all three coefficients (up to about 10 percent for $\alpha=30°$). The slender-airfoil method again predicts these coefficients with surprising accuracy.

In order to further assess the accuracy of the slender-airfoil method, some additional calculations were carried out for the biconvex airfoil at $\alpha=0°$ and $M_0=20$ and 30. The pressure distributions for these cases were calculated by the shock-expansion method, slender-airfoil method ($\gamma=\gamma_a$), and slender-airfoil method ($\gamma=\gamma_i$). These results are presented in figure 25, and it is observed that the use of γ_a rather than γ_i improves the accuracy of the slender-airfoil method. The extent of this improvement in the case of drag coefficient is shown in figure 26; it would appear that predictions of the slender-airfoil method ($\gamma=\gamma_a$) and shock-expansion method are in as good agreement as for ideal-gas flows (see fig. 15). On the basis of these and previous results, it may be concluded, then, that not only does the shock-expansion method retain its range of applicability when air exhibits caloric imperfections, provided γ of the disturbed air is not appreciably less than 1.3, but also the slender-airfoil method ($\gamma=\gamma_a$) retains its range of applicability.

It would be surprising indeed, however, if this conclusion continued to apply as γ of the disturbed fluid approached 1

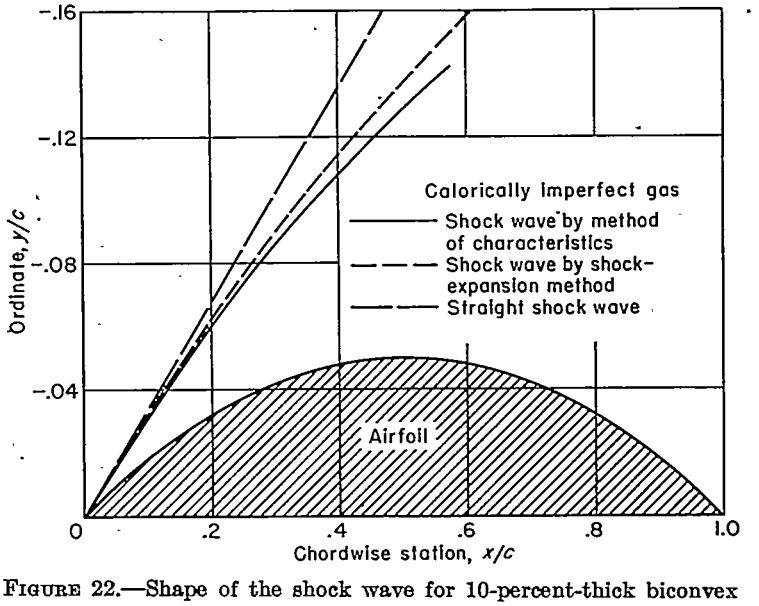

FIGURE 22.—Shape of the shock wave for 10-percent-thick biconvex airfoil section at $\alpha=19.9°$, $M_0=10$, $T_0=500°$ R.

[13] For added ease of calculation the expansion method of Appendix C was employed. This method is also employed in all subsequent calculations of this type since it has been found to yield results differing by less than 1 percent from those obtained by the more tedious graphical integration method.

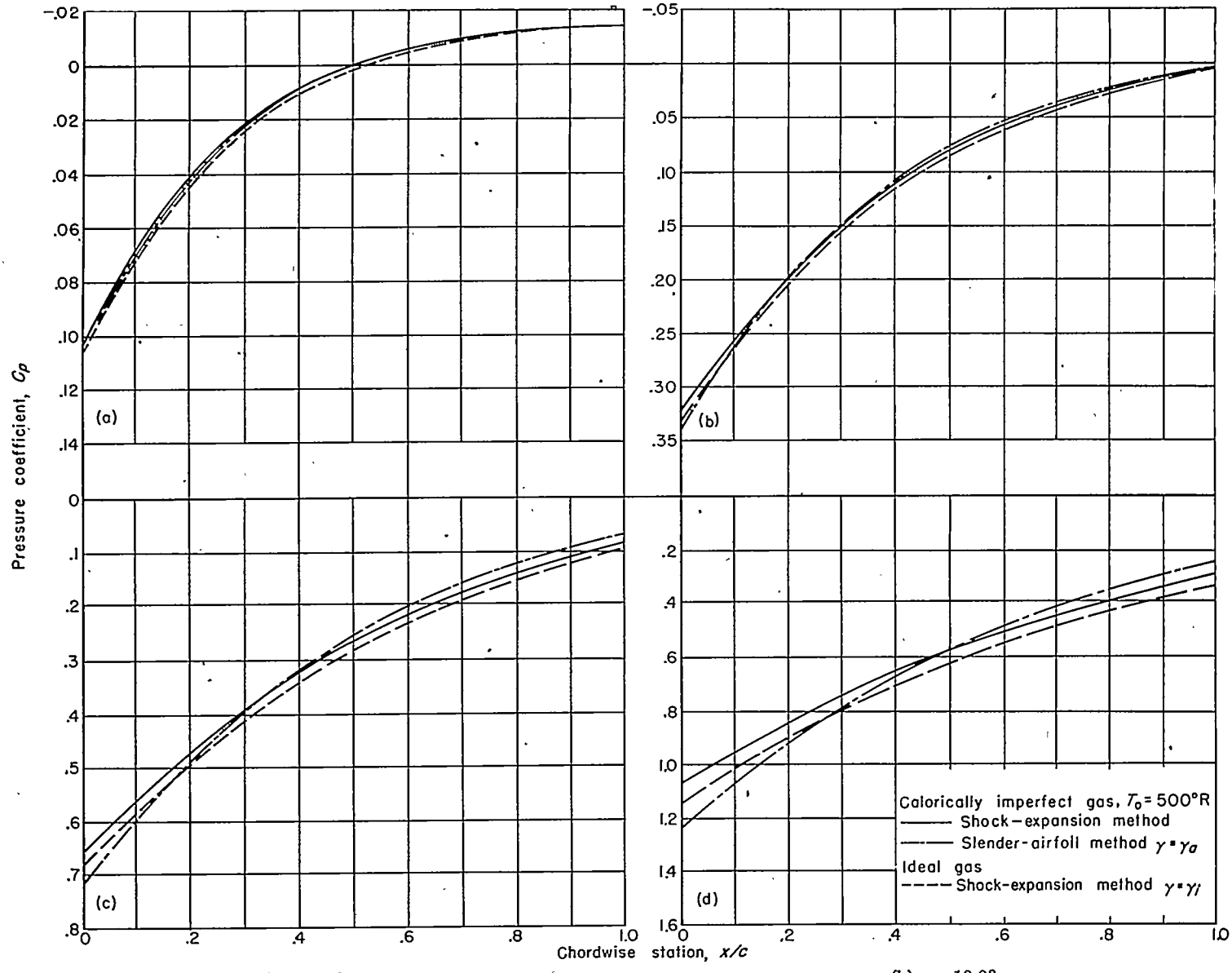

(a) α=0° (b) α=10.0°
(c) α=19.9° (d) α=30.0°

FIGURE 23.—Pressure distribution on lower surface of 10-percent-thick biconvex airfoil section for various angles of attack at M_0=10 and T_0=500° R.

since, as indicated previously, $\frac{\partial\delta/\partial C_1}{\partial\delta/\partial C_2}$ increases with decreasing γ. Although the manner in which γ varies with temperature is not known in this range, some knowledge of these effects can be gained by repeating the ideal-gas calculations for constant values of γ between 1.4 and 1.0.[14] Such calculations have been carried out for infinite Mach number since, in this case, $\frac{\partial\delta/\partial C_1}{\partial\delta/\partial C_2}$ has its maximum value for a given γ, and the results are presented in figure 27. It is seen that except near detachment, the disturbance strength ratio increases with decreasing γ. This increase is slow at first; for example, the value of $\frac{\partial\delta/\partial C_1}{\partial\delta/\partial C_2}$ is still less than 0.1 at γ=1.3. This result is in agreement with the previous conclusion regarding cases where γ is greater than 1.3. However, $\frac{\partial\delta/\partial C_1}{\partial\delta/\partial C_2}$ continues to increase as γ decreases, and, in fact, approaches 1 as γ approaches 1. The effect on pressure distributions of this increase in the strength of the reflected disturbances may also be investigated by using the ideal-gas relationships in combination with appropriate values of γ.

The limiting case of infinite free-stream Mach number and γ=1.0 (for the disturbed fluid, see footnote 14) has already been investigated by Busemann (ref. 21) and more recently by Ivey, Klunker, and Bowen (ref. 22). In this case, as pointed out previously, the shock wave emanating from the leading edge remains attached to the surface downstream of the leading edge (this is easily verified with the oblique-shock-wave equations), and the disturbance flow field is confined to an infinitesimally thin layer adjacent to the surface. In addition, the velocity along a streamline downstream of the shock is constant, as may easily be shown with

[14] Since the enthalpy is negligibly small compared to the mass kinetic energy of the undisturbed fluid at the high Mach numbers of interest and, hence, γ of this fluid does not influence the flow, this approach corresponds to employing an average value of γ for the disturbed fluid.

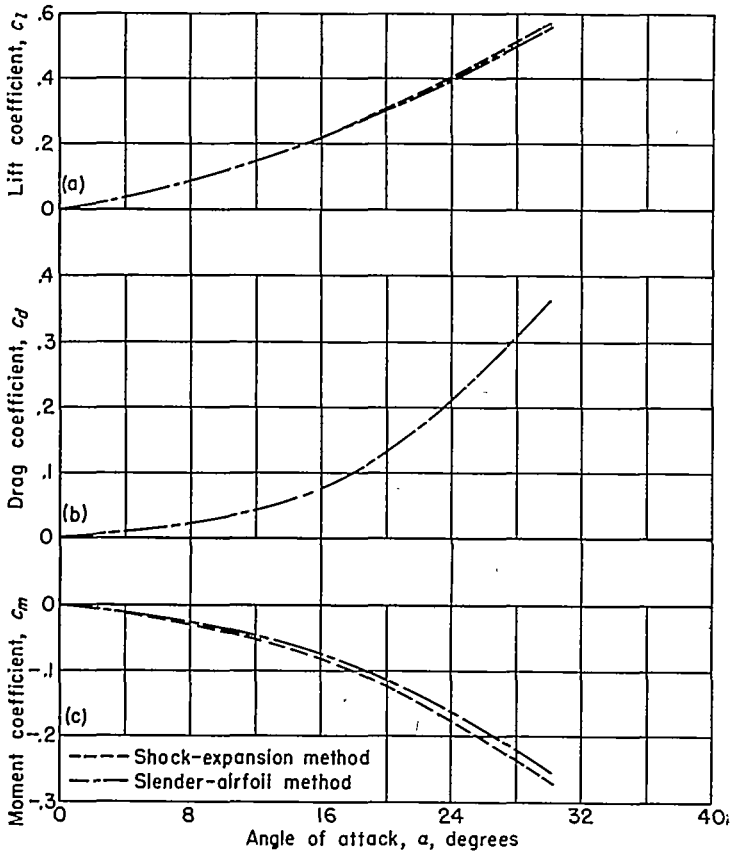

(a) Lift coefficient.
(b) Drag coefficient.
(c) Moment coefficient.

FIGURE 24.—Variation of force and moment coefficients with angle of attack for 10-percent-thick biconvex airfoil section at $M_0=10$, $T_0=500°$ R.

the compatibility equations. Surface pressures therefore become a simple function of airfoil geometry

$$C_p=2\sin^2\delta_S+2\cos\delta_S\frac{d\delta_S}{dx}\int_0^x\sin\delta_S\,dx \qquad (45)$$

varying, to a first approximation, directly with the square of the component of free-stream velocity normal to the surface (i. e., the flow is approximately of the Newtonian corpuscular type). With this theory, then, and the method of characteristics, we can get an idea of both the extent to which changes of γ from 1.4 toward 1 will alter surface pressures, and the accuracy with which the shock-expansion theory predicts the alterations. To this end, figure 28 is presented showing the pressure distributions about the biconvex airfoil at $M_0=\infty$ as calculated by the several methods for different values of γ. It is observed that, whereas the shock-expansion method agrees very closely with the method of characteristics for $\gamma=1.4$, there is a large difference at $\gamma=1.05$. This, of course, is precisely what one would expect from the previous discussion of the disturbance strength ratio. On the other hand, if the two characteristics solutions and the Busemann method are considered in order of decreasing γ, it is indicated that the characteristics solutions approach the Busemann theory as γ approaches 1. For $\gamma=1.0$ and $M_0=\infty$ the shock-expansion method, in turn, predicts a discontinuous pressure distribution with a pressure coefficient equal to that of the Busemann theory at the leading edge but a pressure coefficient of zero at all points downstream of the leading edge. Hence, it may be concluded that when the free-stream Mach number approaches infinity and γ approaches 1, the Busemann method rather than the shock-expansion method for calculating the flow about airfoils should be employed.

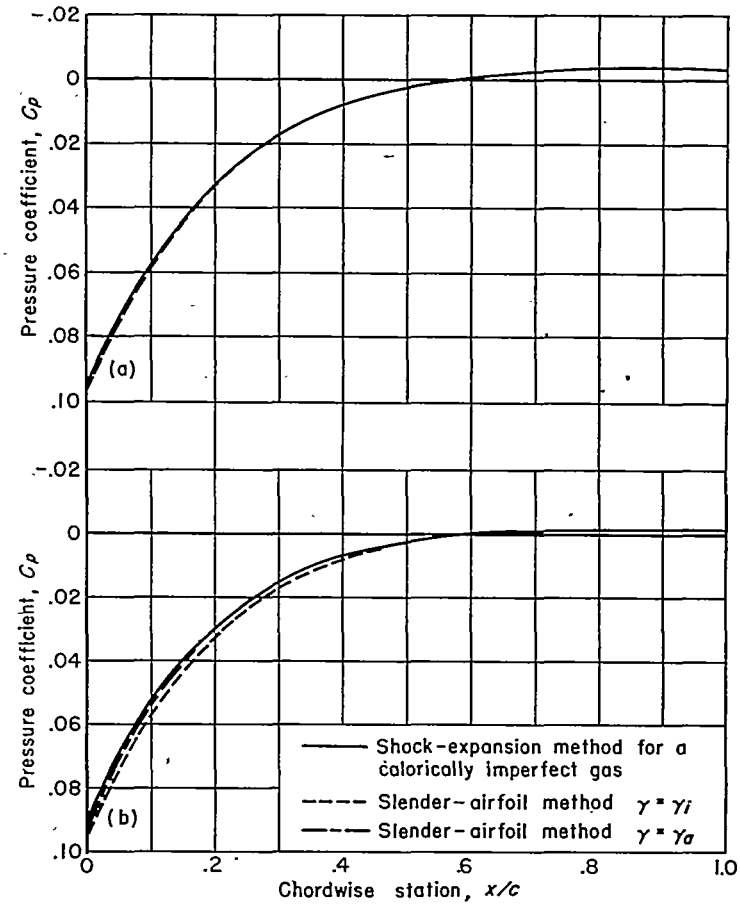

(a) $M_0=20$
(b) $M_0=30$

FIGURE 25.—Pressure distribution on 10-percent-thick biconvex airfoil section at $\alpha=0°$ and $T_0=500°$ R.

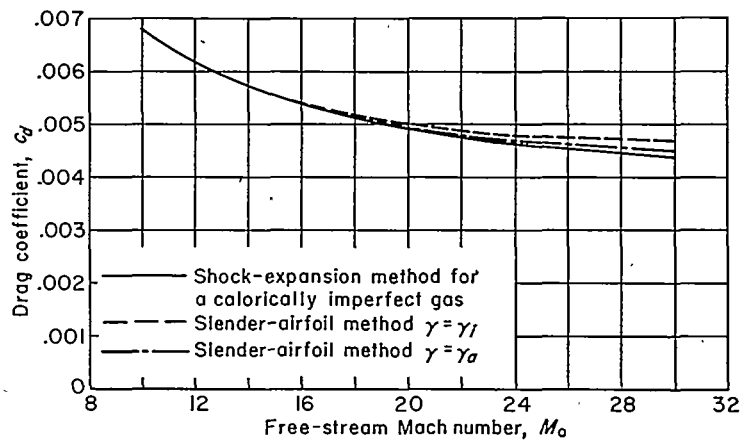

FIGURE 26.—Variation of drag coefficient with Mach number for 10-percent-thick biconvex airfoil section for $\alpha=0°$ and $T_0=500°$ R.

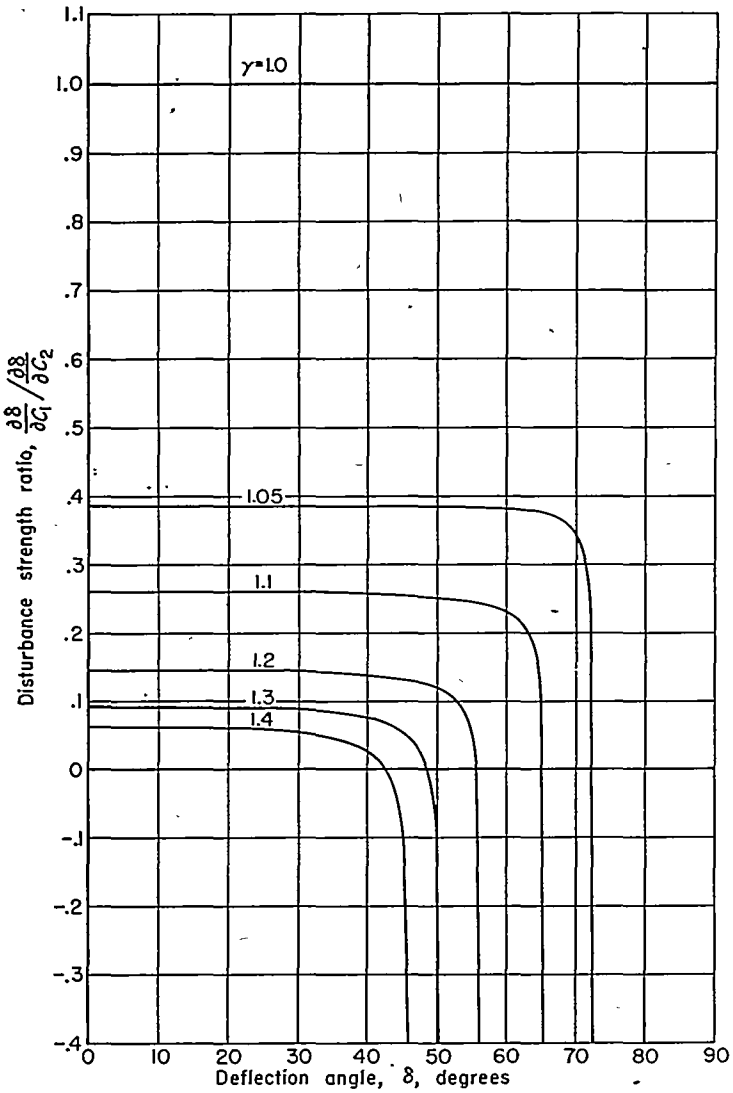

FIGURE 27.—Variation of disturbance strength ratio with deflection angle at infinite free-stream Mach number for various values of γ.

CONCLUSIONS

Inviscid flow about curved airfoils at high supersonic speeds was investigated analytically, first assuming air behaves as an ideal gas, and then assuming it behaves as a thermally perfect, calorically imperfect gas. This study has led to the following conclusions:

1. So long as air behaves as an ideal gas, the shock-expansion method may be used with good accuracy to predict the flow about a curved airfoil up to arbitrarily high Mach numbers, provided the flow deflection angles are about 1° or more below those corresponding to shock detachment. This conclusion applies not only to the determination of surface pressure distributions, but also to the determination of the whole flow field about the airfoil.

2. An approximation to the shock-expansion method, applicable to ideal-gas flows about slender airfoils at high

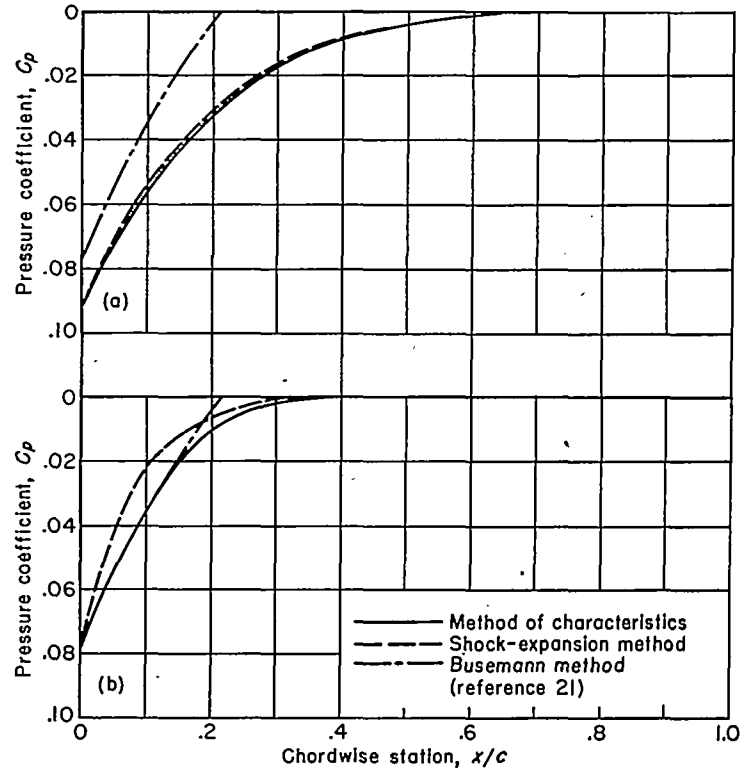

(a) $\gamma=1.4$
(b) $\gamma=1.05$

FIGURE 28.—Pressure distribution on 10-percent-thick biconvex airfoil section at $M_0=\infty$ and $\alpha=0°$.

Mach numbers, predicts pressure coefficients in error by less than 10 percent for Mach numbers above 3 and flow deflection angles up to 25°.

3. So long as caloric imperfections of air do not decrease the ratio of specific heats appreciably below 1.3 (corresponding to air temperatures up to the order of 5,000° R.), the shock-expansion method, generalized to include the effects of these imperfections, is substantially as accurate as for ideal-gas flows. The principal effect of caloric imperfections is to reduce pressure coefficients by as much as 15 percent. The slender-airfoil method can also be made as accurate as for ideal-gas flows by employing an average value of the ratio of specific heats.

4. If the ratio of specific heats approaches 1, as it may at extremely high Mach numbers, the shock-expansion method can be in considerable error. In this case, the Busemann method for flow in the limit of infinite Mach number and specific-heat ratio of 1 applies with reasonable accuracy.

AMES AERONAUTICAL LABORATORY,
NATIONAL ADVISORY COMMITTEE FOR AERONAUTICS,
MOFFETT FIELD, CALIF., *January 9, 1952.*

APPENDIX A

METHOD OF CHARACTERISTICS FOR TWO-DIMENSIONAL FLOW OF A CALORICALLY IMPERFECT GAS

In the application of the method of characteristics for a calorically imperfect, diatomic gas to the particular problem of analyzing the flow about curved two-dimensional airfoils, many of the calculations are identical to those encountered in the solution of any problem where characteristics theory is employed. Since the details of these calculations are well known and well reported (see, e. g., ref. 12), they will not be repeated here.

A lattice-point system with an initial-value, numerical computing procedure will be used. The form of the compatibility equations to be employed was developed previously;[16] however, it is convenient for purposes of calculation to substitute the pressure ratio, p/q_0, into these equations and to rewrite them as difference equations. Equations (12) and (13) are thus reduced to the following forms:

$$(p/q_0)_C-(p/q_0)_A=-\lambda_A(\delta_C-\delta_A) \tag{A1}$$

and

$$(p/q_0)_C-(p/q_0)_B=\lambda_B(\delta_C-\delta_B) \tag{A2}$$

where

$$\lambda=\frac{2\gamma(p/q_0)}{\sin 2\beta} \tag{A3}$$

It is also convenient to employ several reference curves. These curves can be divided into two groups. The general reference curves consist of γ and $\Lambda(T)$ as a function of temperature, T. Equations (14) and (17) are used to determine these curves. A second set of shock-wave reference curves consisting of p/q_0, σ, and δ as a function of temperature, T, are determined by use of equations (18) through (20)—the values of T_0 and M_0 are presumed known.

In the computations three types of points are encountered. These are (1) a point in the flow field between the shock wave and the airfoil surface, (2) a point on the airfoil surface, and (3) a point just downstream of the shock wave. Each one of these types of points requires a slightly different computing procedure and they will be considered in order.

POINT IN THE FLOW FIELD BETWEEN THE SHOCK WAVE AND THE AIRFOIL SURFACE

Figure 29 (a) shows a schematic diagram of the system of points to be considered in these calculations. Point C is the unknown point at the intersection of the first-family characteristic line passing through point A and the second-family characteristic line passing through point B. Six quantities are known at both points A and B, and the problem is to calculate these same quantities at point C. These quantities are x, y, δ, p/q_0, T, and T_σ. The first five quantities are of obvious significance. The sixth, T_σ, is defined as the static temperature, just downstream of the shock wave, on the streamline passing through the point C.

The physical coordinates of the point C(x_C, y_C) may be determined by standard procedures such as those given in reference 12. In order to determine the quantity δ_C, it is necessary to solve equations (A1) and (A2) simultaneously, thus,

$$\delta_C=\frac{\lambda_A\delta_A+\lambda_B\delta_B+(p/q_0)_A-(p/q_0)_B}{\lambda_A+\lambda_B} \tag{A4}$$

Equation (A1) or (A2) is then used to obtain $(p/q_0)_C$.

There remains only the problem of determining T_C and T_{σ_C} at point C. The temperature T_{σ_C} is obviously constant

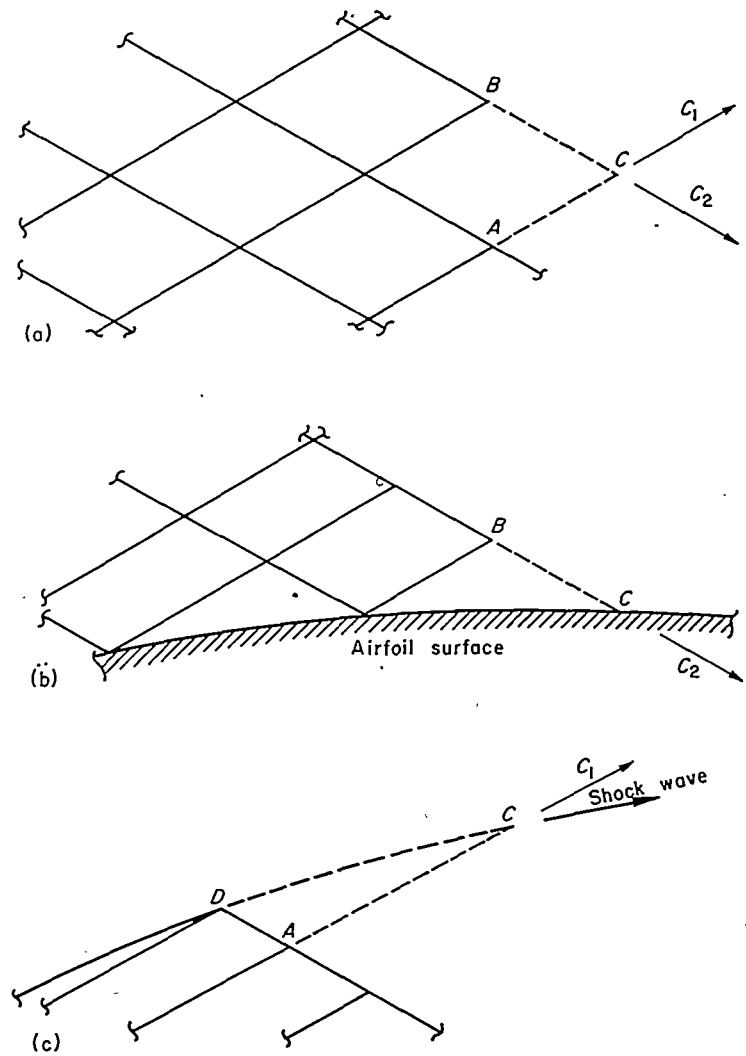

(a) Point in field.
(b) Point on surface.
(c) Point on shock wave.

FIGURE 29.—Diagram of point system in the method of characteristics for the two-dimensional flow of a calorically imperfect gas.

[16] This form of the compatibility equations (in p and δ coordinates) was also used in obtaining some of the characteristics solutions for ideal-gas flows. The majority of these solutions were carried out, however, with the compatibility equations in β, δ, and entropy coordinates, since it was found that greater accuracy was usually obtained for a given net size. In general, the net size employed yielded pressures at from 30 to 35 surface points on an airfoil with a maximum error in the corresponding pressure coefficients equal to less than 1 percent of the pressure coefficient at the leading edge.

along the streamline through C. This quantity may therefore be calculated in the same manner as the entropy is calculated in similar flow fields for ideal-gas processes (see, e. g., ref. 12). Furthermore, since the flow along streamlines downstream of the shock wave is isentropic, equation (16) may be applied in the form

$$\frac{(p/q_0)_C}{(p/q_0)_{\sigma_C}}=\frac{\Lambda(T_{\sigma_C})}{\Lambda(T_C)} \tag{A5}$$

The pressure, $(p/q_0)_{\sigma_C}$, is defined in a manner analogous to T_{σ_C}, and may thus be determined using the shock-wave reference curves and the known value of T_{σ_C}. Similarly, $\Lambda(T_{\sigma_C})$ may be determined from the general reference curves. The only unknown in equation (A5) then is $\Lambda(T_C)$ which may now be calculated. Once $\Lambda(T_C)$ is determined, T_C may be determined by again using the general reference curves. All six quantities, x_C, y_C, δ_C, $(p/q_0)_C$, T_C, and T_{σ_C} have now been determined.

POINT ON THE AIRFOIL SURFACE

Figure 29(b) shows a schematic diagram of the points to be considered in these calculations. The physical coordinates of point C(x_C, y_C) are first calculated by solving simultaneously the equation of the second-family Mach line passing through point B and the equation of the airfoil surface. When x_C and y_C have been determined, δ_C is readily obtained from the equation of the airfoil surface. Equation (A2) is then applied to determine $(p/q_0)_C$.

Since the airfoil surface is a streamline, T_{σ_C} is constant along the surface and may be evaluated at the leading edge. The temperature, T_C, may then be determined using equation (A5) and the previously described procedure. All six quantities, x_C, y_C, $(p/q_0)_C$, δ_C, T_C, and T_{σ_C}, are thus determined.

In the special case of the first point on the airfoil surface downstream of the leading edge, the pressure ratio is calculated using the pressure gradient evaluated at the leading edge. (See section Methods for Calculating the Flow in the Region of the Leading Edge, and Appendix D.) Additional initial points in this region may be calculated by the procedure previously described.

POINT ON THE SHOCK WAVE

Figure 29 (c) shows a schematic diagram of the points to be considered in these calculations. The physical coordinates of point C(x_C, y_C) are first calculated by solving simultaneously the equation of the first-family Mach line passing through point A and the equation of the shock wave linearized at point D, the last known point on the wave. The variation of p/q_0 with δ along the shock wave may be approximated by the relation

$$(p/q_0)_C-(p/q_0)_D=\left[\frac{d(p/q_0)}{d\delta}\right]_\sigma(\delta_C-\delta_D) \tag{A6}$$

In this equation $\left[\frac{d(p/q_0)}{d\delta}\right]_\sigma$ is the rate of change of p/q_0 with δ along the downstream side of the shock wave evaluated at point D. Because of the complicated nature of the shock-wave equations, it is generally easier to evaluate $\left[\frac{d(p/q_0)}{d\delta}\right]_\sigma$ graphically or numerically from the shock-wave reference curves; however, this derivative may also be evaluated from the equations given in Appendix D. Equations (A1) and (A6) are solved simultaneously for δ_C, thus,

$$\delta_C=\frac{\lambda_A\delta_A+\left[\frac{d(p/q_0)}{d\delta}\right]_\sigma\delta_D+(p/q_0)_A-(p/q_0)_D}{\lambda_A+\left[\frac{d(p/q_0)}{d\delta}\right]_\sigma} \tag{A7}$$

when δ_C has been calculated, T_C and, in turn, $(p/q_0)_C$ may be determined from the shock-wave reference curves. Since point C in this case is just downstream of the shock wave, T_C and T_{σ_C} are identical. The six quantities, x_C, y_C, $(p/q_0)_C$, δ_C, T_C, and T_{σ_C} have now been determined.

APPENDIX B

SHOCK-EXPANSION METHOD FOR CALCULATING THE FLOW FIELD ABOUT AN AIRFOIL

An initial-value procedure which is similar to, although markedly simpler than, that associated with the method of characteristics may be employed to carry out this calculation.[16] To illustrate, consider figure 30. With the oblique-shock-wave and expansion equations, all fluid properties at points A, B, D, and so forth, on the airfoil surface may be

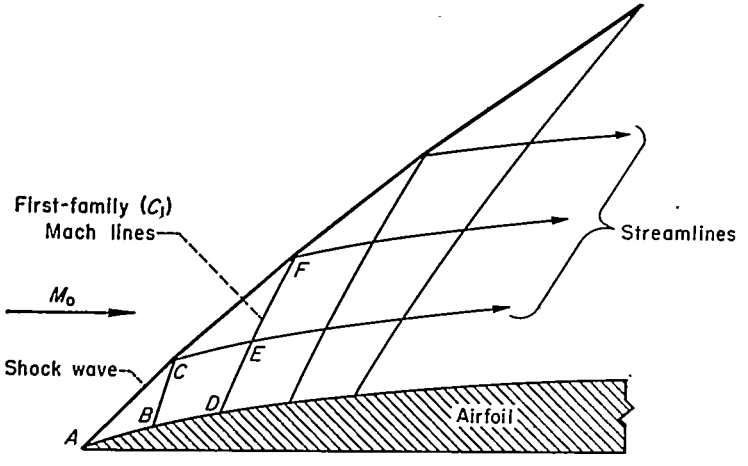

FIGURE 30.—Schematic diagram of shock-expansion method for calculating the flow field about an airfoil.

calculated in the usual manner. If point B is chosen close to point A, the first-family (C_I) Mach line connecting B to point C on the shock wave may be considered straight and inclined at an angle to the free stream equal to $\beta_B+\delta_B$. Similarly, the segment of the shock wave AC may be considered straight and inclined to the free-stream direction at an angle of σ_A. Thus, the physical coordinates of point C may be easily calculated. Since δ is assumed constant along first-family Mach lines, δ_C is equal to δ_B. All fluid properties at point C may be calculated from this known value of δ_C with the oblique-shock-wave equations. In a similar manner, the segment DE of the next first-family Mach line is considered straight and inclined at $\beta_D+\delta_D$, and the streamline joining points C and E is considered straight and inclined at δ_C. The physical coordinates of point E are therefore easily obtained. Since the flow along streamlines downstream of the shock wave is isentropic and since the pressure is also assumed constant along the first-family Mach lines (i. e., $P_E=P_D$), the fluid properties at point E are readily obtained from the known properties at point C, using the isentropic flow relationships. The construction of the remainder of the flow field follows in a similar manner.

As was discussed previously, the assumption that δ is constant along first-family Mach lines is an additional condition which, in general, overdetermines the flow field. It is possible, therefore, to calculate two values of the shock-wave angle at each point on the shock, one assuming δ is constant and one assuming the pressure is constant. These two values will differ slightly and it can be shown that they will bracket the correct value that would be given by the method of characteristics. It is also relatively easy to show that if the change in δ (or p) along C_I given by the corresponding characteristic solution is small,[17] the true value of the shock-wave angle lies just midway between the two values given by the different assumptions. It is apparent then that a closer approximation to the shock-wave shape can be easily obtained by simply averaging the values of shock-wave angle determined by assuming δ is constant and by assuming p is constant. The increase in accuracy is illustrated in figure 31 for the biconvex airfoil at $M_0=\infty$. The averaging procedure gives a shock-wave shape that is closer to that given by the method of characteristics by 60 to 80 percent. The increase in computation time (at least for ideal-gas flows) is negligible. In this regard, it is interesting to note that the shock-expansion solutions require less than 20 percent the computation time of the characteristic solutions.

The shock-expansion method is applicable to the determination of the flow not only in the region adjacent to the airfoil (whether concave or convex), but also in the region downstream of the airfoil; hence, it may, for example, prove useful in downwash studies and the like.

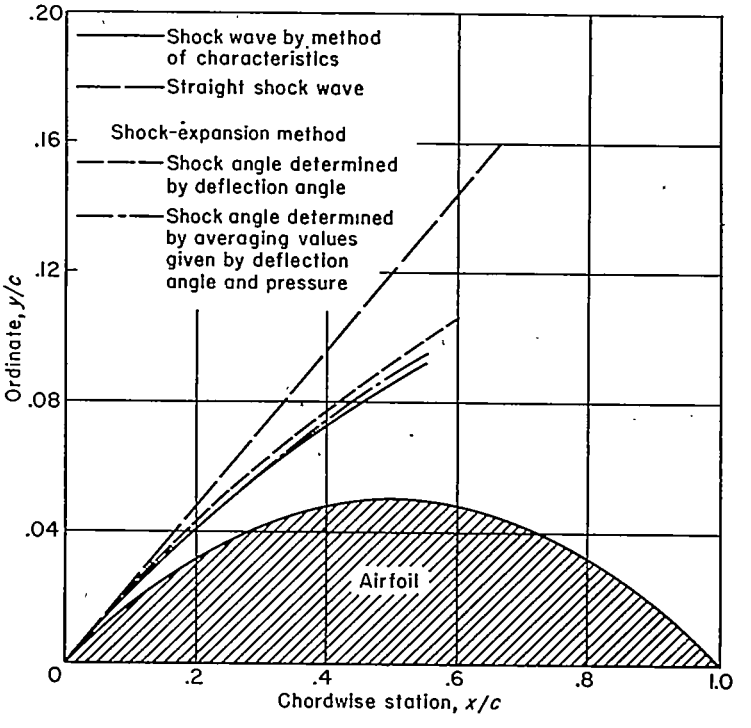

FIGURE 31.—Shape of the shock wave for 10-percent-thick biconvex airfoil section at $\alpha=0°$ and $M_0=\infty$.

[16] It is clear, of course, that an average-value procedure could also be employed. In fact, for the shock-expansion method, an average-value procedure requires very little additional computation since the fluid properties for a system of points can be obtained independently of their physical coordinates. (The difference in the average- or initial-value procedures appears only in computing the physical coordinates.) Thus, the slopes at both ends of a line segment are known before the line is added to the construction. No iteration, as required in characteristic solutions, is necessary in this case.

[17] The necessary assumption here is that $\left(\frac{dP}{d\delta}\right)_{C_2}$ and $\left(\frac{dP}{d\delta}\right)_{\sigma}$ are nearly equal. This is equivalent to the condition that $\frac{\partial\delta/\partial C_1}{\partial\delta/\partial C_2}$ is much less than one. (See eq. (40).)

APPENDIX C

APPROXIMATE SOLUTION FOR PRANDTL-MEYER FLOW OF A CALORICALLY IMPERFECT GAS

The following solution is obtained with an analysis similar to that used in Meyer's original paper (ref. 23). A schematic diagram of the subject flow field is shown in figure 32. It is

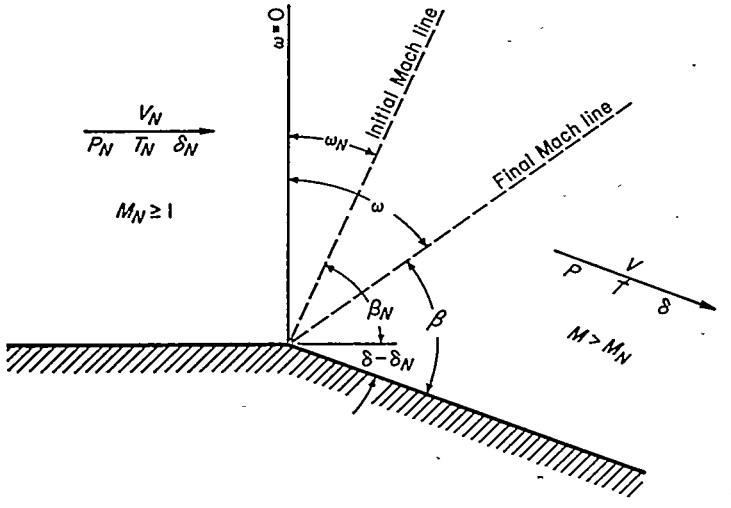

FIGURE 32.—Schematic diagram of Prandtl-Meyer flow around a corner.

evident that the change in flow-inclination angle for Prandtl-Meyer flow can be written as follows:

$$\delta_N - \delta = (\beta_N - \beta) + (\omega_N - \omega) \tag{C1}$$

Since the flow is isentropic, a given value of the local pressure will determine the Mach angle, β. The problem, then, is to evaluate the angle, ω. To this end, the velocity components tangential and normal to the first-family Mach lines may be expressed in the usual manner in terms of a potential φ, thus,

$$u = \frac{\partial \varphi}{\partial r} \tag{C2}$$

$$a = \frac{1}{r}\frac{\partial \varphi}{\partial \omega} \tag{C3}$$

It is clear, however, that these components are functions of ω only; hence, it is convenient to define a new velocity potential which is a function of ω alone. Such a potential is

$$\Phi(\omega) = \frac{\varphi}{r} \tag{C4}$$

The velocity components may then be written in terms of this new potential.

$$u = \Phi \tag{C5}$$

$$a = \Phi_\omega \tag{C6}$$

The resultant velocity is given by the expression

$$V^2 = \Phi^2 + \Phi_\omega^2 \tag{C7}$$

Equation (15), for conservation of energy, may be written in terms of the local temperature as follows:

$$V^2 + 2\left(\frac{\gamma_t}{\gamma_t - 1}\right) RT + 2RT\left(\frac{\theta/T}{e^{\theta/T} - 1}\right) = A^2 \tag{C8}$$

The constant, A, is evaluated at the conditions existing upstream of the expansion region; namely,

$$A^2 = V_N^2 + \left(\frac{2\gamma_t}{\gamma_t - 1}\right) RT_N + 2RT_N\left(\frac{\theta/T_N}{e^{\theta/T_N} - 1}\right) \tag{C9}$$

Equations (C7) and (C8) are then combined to yield

$$\Phi^2 + \Phi_\omega^2 = -2RT\left(\frac{\gamma_t}{\gamma_t - 1} + \frac{\theta/T}{e^{\theta/T} - 1}\right) + A^2 \tag{C10}$$

It was shown previously, however, that

$$a^2 = \gamma RT \tag{C11}$$

Equations (C6), (C10), and (C11) may therefore be combined to obtain the following relationship:

$$\Phi^2 + \Phi_\omega^2\left[1 + \frac{2}{\gamma}\left(\frac{\gamma_t}{\gamma_t - 1} + \frac{\theta/T}{e^{\theta/T} - 1}\right)\right] = A^2 \tag{C12}$$

or

$$\Phi^2 + \Phi_\omega^2\left\{\frac{\gamma_t + 1}{\gamma_t - 1} + \frac{2}{\gamma_t - 1}\left[\frac{\gamma_t}{\gamma} - 1 + \frac{\gamma_t - 1}{\gamma_t}\left(\frac{\gamma_t}{\gamma}\right)\frac{\theta/T}{e^{\theta/T} - 1}\right]\right\} = A^2 \tag{C13}$$

From the imperfect-gas relationship for γ we have

$$\frac{\gamma_t}{\gamma} = \frac{1 + (\gamma_t - 1)\left(\frac{\theta}{T}\right)^2 \frac{e^{\theta/T}}{(e^{\theta/T} - 1)^2}}{1 + \frac{\gamma_t - 1}{\gamma_t}\left(\frac{\theta}{T}\right)^2 \frac{e^{\theta/T}}{(e^{\theta/T} - 1)^2}} \tag{C14}$$

By substitution of this relation into equation (C13) there is then obtained

$$\Phi^2 + \Phi_\omega^2\left[\frac{\gamma_t + 1}{\gamma_t - 1} + \frac{2}{\gamma_t} F\left(\frac{\theta}{T}\right)\right] = A^2 \tag{C15}$$

where

$$F\left(\frac{\theta}{T}\right) = \frac{\theta/T}{e^{\theta/T} - 1}\left\{\frac{1 + (\gamma_t - 1)\frac{(\theta/T)e^{\theta/T}}{e^{\theta/T} - 1}\left[1 + \frac{\theta/T}{e^{\theta/T} - 1}\right]}{1 + \frac{\gamma_t - 1}{\gamma_t}\frac{(\theta/T)^2 e^{\theta/T}}{(e^{\theta/T} - 1)^2}}\right\} \tag{C16}$$

Now

$$\frac{\gamma T}{\gamma_t \theta} = \frac{a^2}{\gamma_t R\theta} \tag{C17}$$

For every value of T/θ there is thus a particular value of $a^2/\gamma_t R\theta$. The function $F(\theta/T)$ is therefore uniquely determined for any value of a^2 since $\gamma_t R\theta$ is, of course, a constant. With this point in mind, let

$$F(\theta/T) = G(a^2/\gamma_t R\theta) \tag{C18}$$

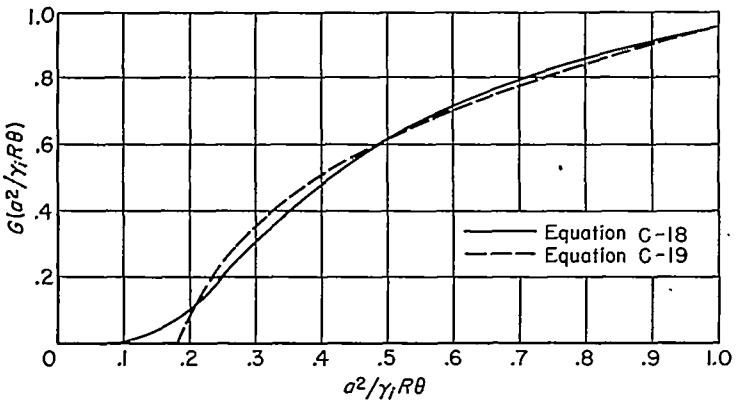

FIGURE 33.—Accuracy of approximation used in Appendix C to obtain solution for Prandtl-Meyer flow of a calorically imperfect gas.

Figure 33 shows $G(a^2/\gamma_t R\theta)$ plotted as a function of $a^2/\gamma_t R\theta$. This curve is approximated with the following simple relation:

$$G(a^2/\gamma_t R\theta)=0.38\frac{a^2}{\gamma_t R\theta}+0.71-\frac{0.14}{a^2/\gamma_t R\theta} \tag{C19}$$

for $0.18<\frac{a^2}{\gamma_t R\theta}<1.0$

and

$$G(a^2/\gamma_t R\theta)=0 \tag{C20}$$

for $0<\frac{a^2}{\gamma_t R\theta}<0.18$

Equation (C19) is also plotted in figure 33 to show the accuracy of this approximation. Consider first the case when G is given by equation (C19) which is written in the form

$$G(a^2/\gamma_t R\theta)=\xi a^2+\mu+\eta\frac{1}{a^2} \tag{C21}$$

where, obviously,

$$\left.\begin{aligned}\xi&=0.38/\gamma_t R\theta\\ \mu&=0.71\\ \eta&=-0.14\,(\gamma_t R\theta)\end{aligned}\right\} \tag{C22}$$

Equation (C21) is substituted into equation (C15) and, with equations (C18) and (C6), the following expression results:

$$\frac{2\xi}{\gamma_t}\Phi_\omega{}^4+\left(\frac{\gamma_t+1}{\gamma_t-1}+\frac{2\mu}{\gamma_t}\right)\Phi_\omega{}^2+\Phi^2+\frac{2\eta}{\gamma_t}-A^2=0 \tag{C23}$$

In order to simplify this equation the following substitutions are made:

$$D^2=\left(\frac{\gamma_t+1}{\gamma_t-1}+\frac{2\mu}{\gamma_t}\right)^2+\frac{8}{\gamma_t}\xi\left(A^2-\frac{2}{\gamma_t}\eta\right) \tag{C24}$$

$$\sin^2\nu=\frac{\frac{8\xi}{\gamma_t}\left(A^2-\frac{2}{\gamma_t}\eta\right)}{D^2} \tag{C25}$$

$$\sin^2\tau=\frac{\frac{8\xi}{\gamma_t}\Phi^2}{D^2} \tag{C26}$$

and

$$\Phi_\omega{}^2=\frac{D^2\cos^2\tau(\tau_\omega)^2}{\frac{8}{\gamma_t}\xi} \tag{C27}$$

Equation (C23) then reduces to

$$\cos^4\tau(\tau_\omega)^4+\frac{4\cos\nu}{D}\cos^2\tau(\tau_\omega)^2+\frac{4\sin^2\tau}{D^2}-\frac{4\sin^2\nu}{D^2}=0 \tag{C28}$$

This equation is solved for τ_ω, thus,

$$\tau_\omega=\sqrt{\frac{2}{D}}\frac{1}{\cos\tau}(\cos\tau-\cos\nu)^{1/2} \tag{C29}$$

or

$$d\omega=\sqrt{\frac{D}{2}}\frac{\cos\tau\,d\tau}{(\cos\tau-\cos\nu)^{1/2}} \tag{C30}$$

This expression is readily integrated to obtain the following equation relating ω to the local velocity:

$$\omega-\omega_N=\sqrt{D}\{2[E(k,z)-E(k,z_N)]-[F(k,z)-F(k,z_N)]\} \tag{C31}$$

where

E elliptic integral of the second kind

F elliptic integral of the first kind

k $\sin\frac{\nu}{2}$ (modulus)

z $\sin^{-1}\left(\frac{\sin\tau/2}{\sin\nu/2}\right)$ (amplitude)

The procedure for calculating corresponding values of the pressure, p, and the deflection angle, δ, is straightforward with the aid of the preceding equations and may be summarized as follows:

1. Calculate A^2 (eq. (C9))
2. Calculate D^2 (eq. (C24))
3. Calculate ν (eq. (C25))
4. Assume a value of T, less than T_N
5. Calculate p (eqs. (16) and (17))
6. Calculate V^2 (eq. (C8))
7. Calculate γ (eq. (C14))
8. Calculate a^2 (or $\Phi_\omega{}^2$) (eq. (C11))
9. Calculate M and, in turn, β from V and a
10. Calculate u^2 (or Φ^2 (eq. (C7))
11. Calculate τ (eq. (C26))
12. Calculate ω (eq. (C31))
13. Calculate δ (eq. (C1))

This procedure is followed so long as the quantity $a^2/\gamma_t R\theta$ is greater than 0.18. (This is equivalent to the temperature being greater than approximately 1,000° R.) For values of $a^2/\gamma_t R\theta$ less than or equal to 0.18 (or temperatures less than about 1,000° R.), G is set equal to zero (see eq. (C20)) In this case, equation (C15) reduces to the same form as for an ideal gas and, therefore, the well-known ideal-gas relationships can be used.

APPENDIX D

EVALUATION OF $(1/K_W)(dP/dW)$, K_σ/K_W, ψ, AND κ

For an ideal gas, the Mach number, Mach angle, shock-wave angle, and pressure ratio can be calculated at the leading edge, using the standard Rankine-Hugoniot shock relations and utilizing the free-stream Mach number and leading-edge deflection angle. With these flow parameters known, the only terms to be determined in equations (38), (39), (40), (43), and (44) are $\left(\frac{dP}{d\delta}\right)_\sigma$ and $\left(\frac{d\delta}{d\sigma}\right)_\sigma$. These derivatives are easily obtained from the shock relations. (See ref. 9.)

$$\left(\frac{dP}{d\delta}\right)_\sigma=\frac{(dP/d\sigma)_\sigma}{(d\delta/d\sigma)_\sigma} \tag{D1}$$

where

$$\left(\frac{dP}{d\sigma}\right)_\sigma=\frac{2\gamma M_0^2 \sin 2\sigma}{\gamma+1} \tag{D2}$$

and

$$\left(\frac{d\delta}{d\sigma}\right)_\sigma=1-\frac{2(\gamma-1)}{\gamma+1}\cos^2(\sigma-\delta)+\sin 2(\sigma-\delta)\cot 2\sigma \tag{D3}$$

By again using the standard forms of the Rankine-Hugoniot shock relations, it is possible to transform equations (38), (39), and (43) (given in the analysis) into

$$\frac{1}{K_W}\frac{dP}{dW}=\frac{\gamma\tan\zeta}{\sin^2\beta}\left[\frac{1+\frac{1}{2}\left(\frac{\cos^2\beta}{\cos^2\zeta}+\frac{1}{M_0^2\sin^2\sigma}\right)}{\frac{\tan^2\zeta}{\tan^2\beta}+\frac{1}{2}\left(\frac{\cos^2\beta}{\cos^2\zeta}+\frac{1}{M_0^2\sin^2\sigma}\right)}\right]\times$$

$$\left[\frac{2\gamma M_0^2\sin^2\sigma-(\gamma-1)}{\gamma+1}\right] \tag{D4}$$

for the surface pressure gradient,

$$\frac{K_\sigma}{K_w}=\frac{\gamma+1}{4\cos\zeta}\left[\frac{1-\frac{\tan^2\zeta}{\tan^2\beta}}{\frac{\tan^2\zeta}{\tan^2\beta}+\frac{1}{2}\left(\frac{\cos^2\beta}{\cos^2\zeta}+\frac{1}{M_0^2\sin^2\sigma}\right)}\right] \tag{D5}$$

for the shock-wave curvature, and

$$\psi=\left[\frac{1+\frac{1}{2}\left(\frac{\cos^2\beta}{\cos^2\zeta}+\frac{1}{M_0^2\sin^2\sigma}\right)}{\frac{\tan^2\zeta}{\tan^2\beta}+\frac{1}{2}\left(\frac{\cos^2\beta}{\cos^2\zeta}+\frac{1}{M_0^2\sin^2\sigma}\right)}\right]\frac{\tan\zeta}{\tan\beta} \tag{D6}$$

for the surface-pressure-gradient ratio. These equations are similar to those given by Schaefer in reference 8 and require less work to compute than equations (38), (39), and (43).

For calorically-imperfect-gas flows, the standard shock relations are obviously not applicable. In this case, the flow parameters at the leading edge can be evaluated using the oblique-shock-wave equations previously presented. (See eqs. (14), (15), (18), (19), and (20).) Since the primary variable in these equations is temperature, the required derivatives are most easily determined by employing the temperature as a parameter.[18] Thus,

$$\left(\frac{dP}{d\delta}\right)_\sigma=\frac{(dP/dT)_\sigma}{(d\delta/dT)_\sigma} \tag{D7}$$

and

$$\left(\frac{d\delta}{d\sigma}\right)_\sigma=\frac{(d\delta/dT)_\sigma}{(d\sigma/dT)_\sigma} \tag{D8}$$

Differentiation of equation (18) yields

$$\left(\frac{dP}{dT}\right)_\sigma=\frac{P^2}{T_\sigma}\frac{T_0(P-1-\gamma_0M_0^2)-M_\sigma T_\sigma^2\left(M_\sigma\frac{d\gamma}{dT}+2\gamma_\sigma\frac{dM}{dT}\right)}{T_\sigma+T_0P^2} \tag{D9}$$

where from equation (15)

$$\frac{dM}{dT}=\left(\frac{-1}{\gamma_\sigma T_\sigma M_\sigma}\right)\left[\frac{M_\sigma^2T_\sigma}{2}\frac{d\gamma}{dT}+\frac{\gamma_\sigma M_\sigma^2}{2}+\right.$$

$$\left.e^{\theta/T_\sigma}\left(\frac{\theta/T_\sigma}{e^{\theta/T_\sigma}-1}\right)^2+\frac{\gamma_t}{\gamma_{t-1}}\right] \tag{D10}$$

and from equation (14)

$$\frac{d\gamma}{dT}=\frac{(\gamma_t-\gamma)(\gamma-1)}{T_\sigma(\gamma_t-1)}\left(2-\frac{\theta}{T_\sigma}\frac{e^{\theta/T_\sigma}+1}{e^{\theta/T_\sigma}-1}\right) \tag{D11}$$

The derivative $\left(\frac{d\delta}{dT}\right)_\sigma$ can be evaluated from equation (20)

$$\left(\frac{d\delta}{dT}\right)_\sigma=\sin^2\delta\left[\frac{\gamma_0M_0^2\tan\sigma\left(\frac{dP}{dT}\right)_\sigma}{(P-1)^2}-\right.$$

$$\left.\left(\frac{\gamma_0M_0^2}{P-1}-1\right)\sec^2\sigma\left(\frac{d\sigma}{dT}\right)_\sigma\right] \tag{D12}$$

where from equation (19)

$$\left(\frac{d\sigma}{dT}\right)_\sigma=$$

$$\frac{csc\,2\sigma\left(\frac{\gamma_\sigma M_\sigma^2T_\sigma}{\gamma_0M_0^2T_0}\right)\left(\frac{2}{M_\sigma}\frac{dM}{dT}+\frac{1}{T_\sigma}+\frac{1}{\gamma_\sigma}\frac{d\gamma}{dT}\right)+\tan\sigma\frac{\rho_0^2}{\rho_\sigma^3}\left(\frac{d\rho}{dT}\right)_\sigma}{\left(\frac{\rho_0}{\rho_\sigma}\right)^2-1} \tag{D13}$$

and from equation (8)

$$\left(\frac{d\rho}{dT}\right)_\sigma=\frac{1}{T_\sigma}\left[\rho_0T_0\left(\frac{dP}{dT}\right)_\sigma-\rho_\sigma\right] \tag{D14}$$

The procedure for calculating $\frac{1}{K_w}\frac{dP}{dW}$, $\frac{K_\sigma}{K_w}$, ψ, and κ is straightforward with the aid of the preceding equations and may be summarized as follows:

1. For any M_0, T_0, δ_N, and K_w choose a value of T_σ/T_0.

[18] The forms of some of the derivatives presented have been somewhat simplified from the forms originally presented in reference 17.

(Fig. 6 or the ideal-gas relations will provide an initial estimate.)

2. Calculate γ_σ (eq. (14))
3. Calculate M_σ (eq. (15))
4. Calculate P_σ (eq. (18))
5. Calculate ρ_0/ρ_σ (eq. (8))
6. Calculate σ (eq. (19))
7. Calculate δ_σ (eq. (20))

If this value of δ_σ is not close enough to the desired value of δ_N, iterate, choosing a new T_σ/T_0.

8. Calculate $\frac{d\gamma}{dT}$ (eq. (D11))
9. Calculate $\frac{dM}{dT}$ (eq. (D10))
10. Calculate $\left(\frac{dP}{dT}\right)_\sigma$ (eq. (D9))
11. Calculate $\left(\frac{d\rho}{dT}\right)_\sigma$ (eq. (D14))
12. Calculate $\left(\frac{d\sigma}{dT}\right)_\sigma$ (eq. (D13))
13. Calculate $\left(\frac{d\delta}{dT}\right)_\sigma$ (eq. (D12))
14. Calculate $\left(\frac{dP}{d\delta}\right)_\sigma$ (eq. (D7))
15. Calculate $\frac{\partial\delta/\partial C_1}{\partial\delta/\partial C_2}$ (eq. (40))
16. Calculate $\frac{1}{K_w}\frac{dP}{dW}$ (eq. (38))
17. Calculate ψ (eq. (43))
18. Calculate $\left(\frac{d\delta}{d\sigma}\right)_\sigma$ (eq. (D8))
19. Calculate $\frac{K_\sigma}{K_w}$ (eq. (39))
20. Calculate κ (eq. (44))

REFERENCES

1. Ackeret, J.: Air Forces on Airfoils Moving Faster than Sound. NACA TM 317, 1925.
2. Busemann, A., and Walchner, O.: Airfoil Characteristics at Supersonic Velocities. British R. T. P. Trans. 1786. (Forschung auf dem gebiete des Ingenieurwesens, vol. 4, no. 2, Mar./Apr. 1933, pp. 87–92.)
3. Epstein, Paul S.: On the Air Resistance of Projectiles. Proceedings of the National Academy of Sciences, vol. 17, 1931, pp. 532–547.
4. Eggers, A. J., Jr.: One-Dimensional Flows of an Imperfect Diatomic Gas. NACA Rep. 959, 1950. (Formerly NACA TN 1861)
5. Ivey, H. Reese, and Cline, Charles W.: Effect of Heat-Capacity Lag on the Flow Through Oblique Shock Waves. NACA TN 2196, 1950.
6. Bethe, H. E., and Teller, E.: Deviations from Thermal Equilibrium in Shock Waves. Ballistic Research Lab. Rept. No. X–117. Aberdeen Proving Ground, Aberdeen, Maryland, 1945.
7. Crocco, Luigi: Singolarita della Corrente Gassosa Iperacustica Nell'Intorno di una Prora a Diedro. L'Aerotecnica, vol. 17, no. 6, June 1937, pp. 519–534.
8. Schaefer, M.: The Relation Between Wall Curvature and Shock Front Curvature in Two-Dimensional Gas Flow. USAF Tech. Rep. F–TS–1202–IA, Jan. 1949.
9. Munk, M. M., and Prim, R. C.: Surface-Pressure Gradient and Shock-Front Curvature at the Edge of a Plane Ogive with Attached Shock Front. Jour. Aero. Sci., vol. 15, no. 11, Nov. 1948, pp. 691–695.
10. Thomas, T. Y.: Calculation of the Curvatures of Attached Shock Waves. Jour. Math. and Phys., vol. 27, no. 4, Jan. 1949, pp. 279–297.
11. Chapman, Dean R.: Airfoil Profiles for Minimum Pressure Drag at Supersonic Velocities—General Analysis With Application to Linearized Supersonic Flow. NACA Rep. 1063, 1952. (Formerly NACA TN 2264)
12. Isenberg, J. S.: The Method of Characteristics in Compressible Flow. Part I (Steady Supersonic Flow) USAF Tech. Rept. F–TR–1173A–ND, Air Materiel Command, Wright Field, Technical Intelligence (Brown University, Graduate Division of Applied Mathematics, A–9–M 11/1), Dec. 1947.
13. Thomas, T. Y.: The Determination of Pressure on Curved Bodies Behind Shocks. Communications on Pure and Applied Mathematics, vol. III, no. 2, June 1950, pp. 103–132.
14. Noyes, Robert N.: Prandtl-Meyer Flow for a Diatomic Gas of Variable Specific Heat. NACA TN 2125, 1950.
15. Tsien, Hsue-shen: Similarity Laws of Hypersonic Flows. Jour. Math. and Phys., vol. 25, no. 3, Oct. 1946, pp. 247–251.
16. Linnell, Richard D.: Two-Dimensional Airfoils in Hypersonic Flows. Jour. Aero. Sci., vol. 16, no. 1, Jan. 1949, pp. 22–30.
17. Kraus, Samuel: An Analysis of Supersonic Flow in the Region of the Leading Edge of Curved Airfoils, Including Charts for Determining Surface-Pressure Gradient and Shock-Wave Curvature. NACA TN 2729, 1952.
18. Lighthill, M. J.: The Flow Behind a Stationary Shock. Philosophical Magazine, ser. 7, vol. 40, Feb. 1949, pp. 214–220.
19. Eggers, A. J., Jr., and Syvertson, Clarence A.: Inviscid Flow About Airfoils at High Supersonic Speeds. NACA TN 2646, 1952.
20. Rand, Robert C.: Prandtl-Meyer Flow Behind a Curved Shock Wave. Jour. Math. and Phys., vol. 29, no. 2, July 1950, pp. 124–132.
21. Busemann, A.: Flussigkeits-und Gasbewegung. Handworterbuch der Naturwissenschaften, Zweite Auflage, Gustav. Fischer, Jena, 1933, pp. 266–279.
22. Ivey, H. Reese, Klunker, E. Bernard, and Bowen, Edward N.: A Method for Determining the Aerodynamic Characteristics of Two- and Three-Dimensional Shapes at Hypersonic Speeds. NACA TN 1613, 1948.
23. Meyer, Th.: The Two Dimensional Phenomena of Motion in a Gas Flowing at Supersonic Velocity. Cornell Research Foundation, Inc., Buffalo, New York, Aug. 1945. (Translation from: Mitteilungen über Forschungsarbeiten auf dem Gebiete des Ingenieurwesens, Heft 62, 1908, pp. 31–67.)

TABLE I.—FUNCTIONS FOR SLENDER-AIRFOIL METHOD

$M_0\delta_N$	$\gamma=\gamma_i$		γ_a	$\gamma=\gamma_a$		$M_0\delta_N$	$\gamma=\gamma_i$		γ_a	$\gamma=\gamma_a$	
	$g(M_0\delta_N)$	$f(M_0\delta_N)$		$g(M_0\delta_N)$	$f(M_0\delta_N)$		$g(M_0\delta_N)$	$f(M_0\delta_N)$		$g(M_0\delta_N)$	$f(M_0\delta_N)$
0	1.000	0	1.400	1.000	0			0			0
.05	1.072	.009901	1.400	1.072	.009897	5.2	47.56	.3487	1.348	44.91	.3275
.10	1.148	.01961	1.400	1.148	.01959	5.4	51.13	.3506	1.347	48.23	.3292
.15	1.230	.02912	1.400	1.230	.02909	5.6	54.82	.3523	1.347	51.68	.3309
.20	1.316	.03845	1.400	1.316	.03841	5.8	58.66	.3539	1.346	55.26	.3323
.25	1.406	.04760	1.400	1.406	.04755	6.0	62.62	.3553	1.346	58.96	.3337
.30	1.502	.05656	1.399	1.502	.05649	6.2	66.73	.3566	1.346	62.79	.3350
.35	1.604	.06537	1.399	1.603	.06524	6.4	70.96	.3578	1.345	66.77	.3363
.40	1.710	.07393	1.399	1.710	.07380	6.6	75.33	.3589			
.45	1.823	.08235	1.399	1.822	.08220	6.8	79.83	.3600			
.50	1.941	.09058	1.399	1.940	.09040	7.0	84.47	.3610			
.55	2.065	.09863	1.399	2.064	.09841	7.2	89.24	.3618			
.60	2.195	.1071	1.399	2.194	.1062	7.4	94.14	.3626			
.65	2.332	.1142	1.399	2.330	.1139	7.6	99.19	.3633			
.70	2.474	.1217	1.399	2.473	.1213	7.8	104.4	.3640			
.75	2.624	.1290	1.398	2.622	.1286	8.0	109.7	.3647			
.80	2.780	.1362	1.398	2.777	.1356	8.5	123.5	.3661			
.85	2.943	.1431	1.398	2.939	.1425	9.0	138.2	.3673			
.90	3.112	.1499	1.398	3.108	.1492	9.5	153.8	.3684			
.95	3.289	.1565	1.398	3.284	.1557	10.0	170.2	.3693			
1.00	3.473	.1630	1.397	3.466	.1620	10.5	187.4	.3701			
1.1	3.862	.1753	1.396	3.852	.1740	11.0	205.4	.3707			
1.2	4.280	.1869	1.396	4.268	.1853	11.5	224.3	.3714			
1.3	4.728	.1978	1.395	4.708	.1958	12.0	244.1	.3719			
1.4	5.206	.2084	1.393	5.179	.2056	12.5	264.7	.3723			
1.5	5.715	.2178	1.392	5.679	.2147	13.0	286.1	.3727			
1.6	6.256	.2269	1.391	6.207	.2232	13.5	308.3	.3731			
1.7	6.827	.2354	1.389	6.764	.2309	14.0	331.4	.3735			
1.8	7.431	.2433	1.388	7.349	.2381	14.5	355.4	.3738			
1.9	8.066	.2507	1.386	7.962	.2447	15.0	380.2	.3740			
2.0	8.734	.2577	1.384	8.605	.2508	16.0	432.3	.3745			
2.1	9.411	.2646	1.382	9.274	.2564	17.0	487.7	.3749			
2.2	10.17	.2702	1.380	9.973	.2616	18.0	546.5	.3752			
2.3	10.93	.2759	1.378	10.70	.2664	19.0	608.6	.3755			
2.4	11.73	.2812	1.376	11.46	.2709	20.0	674.2	.3757			
2.5	12.56	.2862	1.374	12.24	.2749	22.0	815.3	.3761			
2.6	13.42	.2908	1.372	13.06	.2788	24.0	969.8	.3764			
2.7	14.32	.2951	1.370	13.90	.2823	26.0	1138	.3766			
2.8	15.25	.2992	1.369	14.77	.2856	28.0	1319	.3768			
2.9	16.21	.3030	1.367	15.68	.2887	30.0	1514	.3770			
3.0	17.21	.3066	1.365	16.61	.2916	35.0	2060	.3772			
3.2	19.30	.3130	1.362	18.56	.2968	40.0	2690	.3774			
3.4	21.52	.3187	1.360	20.64	.3015	45.0	3404	.3775			
3.6	23.88	.3237	1.358	22.83	.3057	50.0	4202	.3776			
3.8	26.37	.3280	1.356	25.16	.3094	60.0	6050	.3777			
4.0	29.00	.3322	1.354	27.60	.3128	70.0	8233	.3778			
4.2	31.76	.3358	1.352	30.17	.3158	80.0	10750	.3778			
4.4	34.65	.3389	1.351	32.86	.3186	90.0	13610	.3779			
4.6	37.68	.3418	1.350	35.68	.3211	100.0	16800	.3779			
4.8	40.84	.3443	1.349	38.63	.3234	∞	∞	.3780			
5.0	44.14	.3466	1.349	41.70	.3255						

TABLE II.—SURFACE PRESSURE GRADIENT, $\frac{1}{K_w}\frac{dP}{dW}$

δ_N \ M_0	1.5	2.0	3.0	4.0	5.0	6.0	8.0	10.0	15.0	20.0	∞
0°	2.817	3.233	4.455	5.784	7.144	8.519	11.29	14.07	21.05	28.04	∞
2.0°	3.089	3.530	5.038	6.809	8.757	10.87	15.59	20.99	37.78	59.81	∞
5.0°	3.615	4.014	6.008	8.577	11.64	15.20	23.94	35.02	74.01	130.2	∞
7.5°	4.298	4.458	6.896	10.24	14.41	19.45	32.30	49.10	109.3	195.9	∞
10.0°	5.878	4.950	7.849	12.05	17.46	24.12	41.43	64.23	145.7	261.6	∞
15.0°		6.185	9.908	15.96	24.00	34.06	60.32	94.76	216.1	387.1	∞
20.0°		8.765	12.12	19.99	30.60	43.87	78.34	123.2	280.2	500.7	∞
25.0°			14.56	23.94	36.80	52.88	94.44	148.3	336.2	599.6	∞
30.0°			18.25	27.94	42.54	60.91	108.3	169.7	383.4	682.9	∞
35.0°				33.89	48.83	68.80	120.9	188.5	423.8	753.5	∞
40.0°					71.76	84.90	139.2	212.8	471.1	833.8	∞
45.0°									1727.	1711.	∞

TABLE III.—SURFACE-PRESSURE-GRADIENT RATIO, ψ

δ_N \ M_0	1.5	2.0	3.0	4.0	5.0	6.0	8.0	10.0	15.0	20.0	∞
0°	1.000	1.000	1.000	1.000	1.000	1.000	1.000	1.000	1.000	1.000	0.8820
2.0°	1.000	1.000	1.000	1.000	.9999	.9998	.9996	.9993	.9976	.9948	.8820
5.0°	1.000	1.000	.9998	.9994	.9987	.9978	.9950	.9910	.9773	.9619	.8822
7.5°	1.001	1.000	.9995	.9981	.9961	.9935	.9864	.9777	.9550	.9362	.8825
10.0°	.9978	1.001	.9988	.9959	.9920	.9870	.9754	.9631	.9369	.9198	.8830
15.0°		1.006	.9970	.9895	.9807	.9715	.9538	.9392	.9158	.9041	.8846
20.0°		1.025	.9958	.9824	.9696	.9578	.9386	.9253	.9071	.8991	.8871
25.0°			.9997	.9783	.9623	.9493	.9309	.9194	.9052	.8994	.8911
30.0°			1.025	.9825	.9622	.9482	.9305	.9203	.9087	.9042	.8979
35.0°				1.016	.9787	.9603	.9407	.9307	.9199	.9158	.9104
40.0°					1.114	1.028	.9835	.9672	.9523	.9472	.9407
45.0°									1.737	1.325	1.188

TABLE IV.—SHOCK-WAVE CURVATURE, K_s/K_∞

δ_N \ M_0	1.5	2.0	3.0	4.0	5.0	6.0	8.0	10.0	15.0	20.0	∞
0°	0	0	0	0	0	0	0	0	0	0	0.8000
2.0°	.06597	.04547	.04805	.05767	.06891	.08080	.1054	.1305	.1931	.2537	.8003
5.0°	.1951	.1175	.1212	.1450	.1728	.2017	.2598	.3155	.4357	.5264	.8018
7.5°	.3698	.1827	.1827	.2170	.2566	.2969	.3733	.4406	.5653	.6417	.8042
10.0°	.7988	.2553	.2447	.2869	.3354	.3829	.4676	.5356	.6460	.7042	.8077
15.0°		.4487	.3704	.4183	.4737	.5244	.6044	.6597	.7345	.7677	.8181
20.0°		9.191	.5051	.5399	.5894	.6332	.6970	.7371	.7803	.8064	.8352
25.0°			.6756	.6634	.6956	.7271	.7723	.7997	.8318	.8445	.8621
30.0°			1.014	.8222	.8168	.8294	.8536	.8696	.8835	.8961	.9064
35.0°				1.168	1.021	.9890	.9774	.9779	.9818	.9840	.9875
40.0°					2.040	1.492	1.293	1.240	1.202	1.191	1.179
45.0°									7.668	3.829	2.811

TABLE V.—SHOCK-WAVE-CURVATURE RATIO, κ

δ_N \ M_0	1.5	2.0	3.0	4.0	5.0	6.0	8.0	10.0	15.0	20.0	∞
0°	1.000	1.000	1.000	1.000	1.000	1.000	1.000	1.000	1.000	1.000	1.072
2.0°	.9997	.9998	1.000	1.000	1.001	1.001	1.002	1.003	1.007	1.012	1.072
5.0°	.9984	.9992	1.001	1.002	1.004	1.006	1.011	1.017	1.030	1.040	1.072
7.5°	.9970	.9983	1.002	1.005	1.009	1.013	1.021	1.029	1.044	1.053	1.071
10.0°	1.002	.9968	1.003	1.009	1.014	1.020	1.030	1.038	1.052	1.059	1.071
15.0°		.9912	1.005	1.015	1.024	1.031	1.042	1.049	1.059	1.063	1.069
20.0°		.9795	1.005	1.019	1.029	1.037	1.047	1.053	1.060	1.063	1.067
25.0°			1.000	1.019	1.031	1.039	1.048	1.053	1.058	1.060	1.063
30.0°			.9830	1.013	1.027	1.035	1.044	1.048	1.053	1.055	1.057
35.0°				.9909	1.012	1.023	1.034	1.039	1.044	1.045	1.048
40.0°					.9587	.9879	1.008	1.016	1.023	1.025	1.028
45.0°									.8854	.9242	.9475

TABLE VI.—SURFACE PRESSURE GRADIENT, SURFACE-PRESSURE-GRADIENT RATIO, SHOCK-WAVE CURVATURE, AND SHOCK-WAVE-CURVATURE RATIO FOR A CALORICALLY IMPERFECT, DIATOMIC GAS

[T_0=500° Rankine]

M_0	δ°	T_s/T_0	$\frac{1}{K_\infty}\frac{dP}{dW}$	ψ	K_s/K_∞	κ
3	30.48	2.01200	18.36	1.026	1.021	0.9828
5	8.042	1.32750	15.04	.9954	.2732	1.010
5	15.36	1.75357	24.38	.9796	.4773	1.025
5	20.48	2.13800	30.94	.9675	.5866	1.031
5	26.01	2.62500	37.39	.9577	.6908	1.034
5	31.09	3.12700	42.63	.9549	.7986	1.031
5	37.30	3.81250	49.50	.9725	1.041	1.015
5	41.01	4.30000	60.76	1.042	1.571	.9827
10	10.01	2.10800	63.86	.9621	.5265	1.040
10	10.38	2.17000	66.07	.9598	.5373	1.041
10	20.52	4.40000	123.6	.9112	.7132	1.062
10	27.61	6.45000	156.2	.8932	.7922	1.065
10	31.27	7.64000	169.8	.8886	.8383	1.064
10	40.18	[a] 10.87500	195.0	.8969	1.018	1.050
10	42.98	[a] 12.00000	204.1	.9128	1.151	1.039
15	5.230	1.77500	76.83	.9750	.4454	1.032
15	10.49	3.25000	150.5	.9283	.6363	1.057
15	16.31	5.60000	229.5	.8936	.7260	1.070
15	22.26	8.70000	301.4	.8733	.7834	1.074
15	28.65	[a] 12.75000	364.5	.8630	.8391	1.074
20	5.122	2.15000	132.4	.9594	.5242	1.042
20	10.67	4.70000	274.2	.9027	.6923	1.068
20	16.53	8.70000	417.0	.8706	.7648	1.077
20	20.98	[a] 12.60000	514.4	.8579	.8011	1.079
20	32.51	[a] 25.80000	705.0	.8490	.8914	1.075
20	39.15	[a] 35.00000	771.1	.8571	.9861	1.066

[a] Values of the temperature greater than 5,000° R. downstream of the shock wave.